Department
Chemie und Pharmazie

FRIEDRICH-ALEXANDER
UNIVERSITÄT
ERLANGEN-NÜRNBERG

NATURWISSENSCHAFTLICHE
FAKULTÄT

Surface Characterisation of Ionic Liquid Systems and *in situ* Monitoring of Liquid-Phase Reactions by X-ray Photoelectron Spectroscopy

Oberflächencharakterisierung Ionischer Flüssigkeitssysteme und *in situ* Verfolgung von Flüssig-Phasen Reaktionen mittels Röntgen-Photoelektronenspektroskopie

Der Naturwissenschaftlichen Fakultät der
Friedrich-Alexander-Universität Erlangen-Nürnberg

zur Erlangung des Doktorgrades Dr. rer. nat.

vorgelegt von

Claudia Kolbeck

aus Illertissen

Als Dissertation genehmigt
durch die Naturwissenschaftliche Fakultät
der Friedrich-Alexander-Universität Erlangen-Nürnberg

Tag der mündlichen Prüfung: 19.07.2012

Vorsitzende/r der Promotionskommission: Prof. Dr. Rainer Fink
Erstberichterstatter/in: Prof. Dr. Hans-Peter Steinrück
Zweitberichterstatter/in: Prof. Dr. Jörg Libuda

Contents

Detailed list of papers in Appendix

[P1] K. R. J. Lovelock, **C. Kolbeck**, T. Cremer, N. Paape, P. S. Schulz, P. Wasserscheid, F. Maier, H.-P. Steinrück
Influence of Different Substituents on the Surface Composition of Ionic Liquids Studied Using ARXPS
J. Phys. Chem. B 113 (2009) 2854-2864.

[P2] F. Maier, T. Cremer, **C. Kolbeck**, K. R. J. Lovelock, N. Paape, P. S. Schulz, P. Wasserscheid, H.-P. Steinrück
Insights into the Surface Composition and Enrichment Effects of Ionic Liquids and Ionic Liquid Mixtures
Phys. Chem. Chem. Phys. 12 (2010) 1905-1915.

[P3] **C. Kolbeck**, J. Lehmann, K. R. J. Lovelock, T. Cremer, N. Paape, P. Wasserscheid, A. P. Fröba, F. Maier, H.-P. Steinrück
Density and Surface Tension of Ionic Liquids
J. Phys. Chem. B 114 (2010) 17025-17036.

[P4] **C. Kolbeck**, N. Paape, T. Cremer, P. S. Schulz, F. Maier, H.-P. Steinrück, P. Wasserscheid
Ligand Effects on the Surface Composition of Rh-Containing Ionic Liquid Solutions Used in Hydroformylation Catalysis
Chem. Eur. J. 16 (2010) 12083-12087.

[P5] **C. Kolbeck**, I. Niedermaier, N. Taccardi, P. S. Schulz, F. Maier, P. Wasserscheid, H.-P. Steinrück
Monitoring of Liquid-Phase Organic Reactions by Photoelectron Spectroscopy
Angew. Chem. Int. Ed. 51 (2012) 2610-2613.

[P6] I. Niedermaier, **C. Kolbeck**, N. Taccardi, P. S. Schulz, J. Li, T. Drewello, P. Wasserscheid, H.-P. Steinrück, F. Maier
Organic Reactions in Ionic Liquids Studied by in Situ XPS
ChemPhysChem 13 (2012) 1725-1735.

[P7] **C. Kolbeck**, N. Taccardi, N. Paape, P. S. Schulz, P. Wasserscheid, H.-P. Steinrück, F. Maier
Redox chemistry, solubility, and surface distribution of Pt(II) and Pt(IV) complexes dissolved in ionic liquids
J. Mol. Liq. doi:10.1016/j.molliq.2013.07.007.

1. Introduction

Ionic liquids (ILs) form a subclass of molten salts and are characterised by a melting point below 100 °C. In contrast to conventional salts, like NaCl, ILs exhibit comparably weak Coulomb interactions as they are comprised of ions with relatively large molecular volume and an asymmetric charge distribution[1]; in Figure 1.1, some typical IL ions are depicted. ILs possess also other unique physico-chemical properties such as unusual solvation and miscibility properties[2], a large temperature-range in its molten state[3], a large electro-chemical window, extremely low volatility[4, 5], low flammability[6], electroconductivity[7], *etc*. These properties are tuneable by combining different ions or by introducing alkyl chains or functional groups at the cation or the anion (some authors speak about over 10^{18} possible combinations[8]). Functionalised ILs, which are tailored for a specific application, are called ‘‘task specific ionic liquids’’ (TSILs).[9]

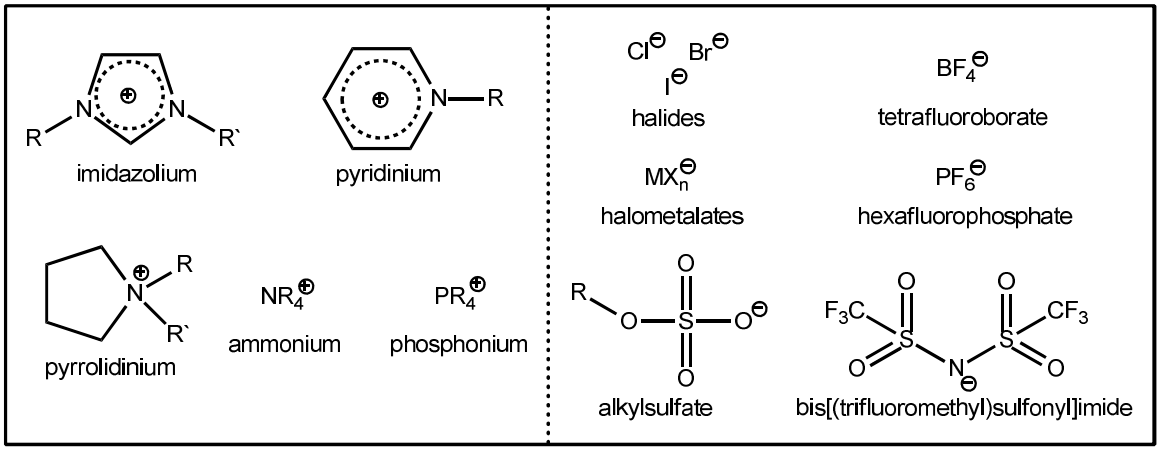

Figure 1.1. Some typical IL cations and anions.

Due to the structural diversity of ILs and their unique physico-chemical properties, ILs have attained strongly increasing scientific attention in the last two decades.[10] ILs are applied in catalysis[11, 12], electrochemistry[13], analytics[14], tribology[15], and as ‘‘engineering fluids’’ (*e.g.*, in separation technologies[16]). Furthermore, the first industrial application was employed in 2002 by BASF with the BASIL process (Biphasic Acid Scavenging utilising Ionic Liquids).[17]

In all of these applications the interface of ILs plays a major role. A molecular understanding of relevant processes occurring at the interfaces involved, such as the surface, is thus of fundamental value. One specific motivation for fundamental research on IL

interfaces stems from applications in heterogeneous catalysis, particular in the Supported Ionic Liquid Phase (SILP) catalysis. The SILP concept was invented in the year 2002 by Mehnert *et al.* and combines the advantages of highly product- and stereo-selective homogeneous catalysis and heterogeneous catalysis, where an easy separation of catalyst and products and the utilisation of a fixed-bed reactor is possible.[18] A schematic drawing of the SILP system is depicted in Figure 1.2[19]: Porous nanoparticles are coated with a thin IL layer, with the catalytically active metal complex dissolved in the IL film. Reagents from the gas phase (or a second liquid phase) penetrate the gas/IL (liquid/IL) interface and diffuse to the catalyst. After the reaction, the products are transferred back into the gas (second liquid) phase.

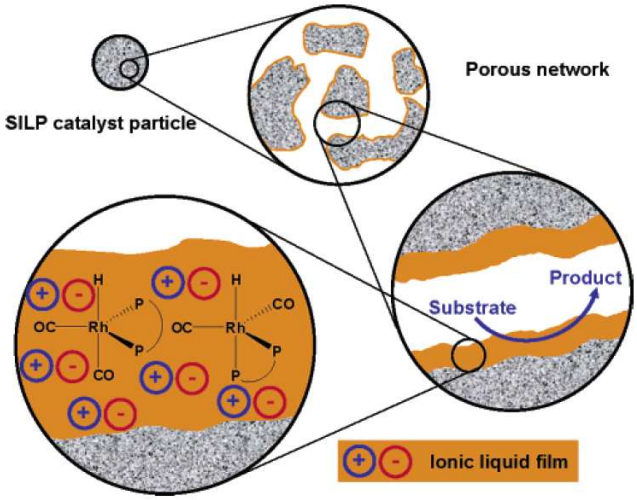

Figure 1.2. Schematic drawing of the Supported Ionic Liquid Phase (SILP) catalysis.[19]

To understand the processes at the IL surface in SILP catalysis, first of all the surface properties of neat ILs have to be considered (Chapter 3). While the ‘‘bulk’’ properties of common ILs have received considerable attention in the past, ‘‘ionic liquid surface science’’, *i.e.*, the investigation of their surface and interface properties just started a few years ago.[20-22] In order to explain fundamental macroscopic surface properties such as surface tension, an understanding of the liquid/vapour interface on a molecular level is vital. Due to the unbalanced forces, which are present as a result of the non-isotropic environment, the chemical composition of the near-surface region and the molecular arrangement at the surface can be different to that in the bulk.

For this purpose, various working groups characterised ILs with different surface-sensitive methods (see Chapter 3 for a detailed list). In this work, angle-resolved X-ray photoelectron spectroscopy (ARXPS) was utilised, as this technique enables a quantitative and qualitative analysis of the sample surface.[23] Commonly, XPS is considered a powerful

surface-sensitive method for the detailed study of solid surfaces and of processes occurring at solid surfaces under ultra-high vacuum (UHV) conditions. The fact that most liquids simply evaporate in UHV due to their comparably high vapour pressures, renders them unsuitable for conventional XPS setups. However, ionic liquids (ILs) present an exception to this restriction as they possess extremely low vapour pressures.[4, 5] Thus XPS can be used to provide additional information concerning the atomistic understanding of surface properties of liquids in general.

Molecular dynamic simulations (MDS) of 1-alkyl-3-methylimidazolium $[C_nC_1Im]^+$ ILs with $n \geq 4$ have shown the formation of polar regions (comprised of the anion and cationic head groups) and non-polar regions (comprised of the alkyl chains) in the bulk.[24, 25] In Chapter 3.1, we show that this behaviour is also reflected at the surface of $[C_nC_1Im][Tf_2N]$ with $n \geq 4$: for these ILs the alkyl chains tend to stick out towards the vacuum, forming an aliphatic overlayer above a polar sublayer, consisting of the anions and the cationic head groups. Chapter 3.3 addresses the influence of functional groups, which are implemented in the alkyl chain of the imidazolium ring, on the surface orientation. While the introduction of fluorine, chlorine or tertiary amine into the alkyl chain does not change the orientation of the chain towards the vacuum, the implementation of ethylene glycol groups leads to an isotropic arrangement at the surface. This isotropy is ascribed to the formation of inter- and intramolecular hydrogen bonds between the ether-oxygen atoms and the acidic H-atoms of the imidazolium ring.[26, 27]

The obtained knowledge about the surface orientation is used, in combination with literature data on the intermolecular interaction energies, to explain trends in the surface tension of neat ILs. The dependence of the surface tension on the alkyl chain length is probed for the system $[C_nC_1Im][Tf_2N]$ (n = 1, 2, 4, 6, 8, 10, 12), where a decrease of the surface tension with increasing alkyl chain length is observed (Chapter 3.1). In contrast to this distinct correlation, variation of the anion in the system $[C_8C_1Im]X$ does not lead to a clear trend (Chapter 3.2). However, by dividing the 12 different studied ILs in sub-groups, which are comprised of ILs with similar chemical structure of the anions (*e.g.*, halides), leads to the observation of trends for the values of the surface tension within these sub-groups.

When considering the SILP system, an enrichment of the catalyst at the surface is preferable, as the diffusion path ways of the reagents and products between the interface and the reactive species is minimised. To understand the driving force of such enrichment effects, the surface composition of binary IL mixtures and IL solutions is regarded in Chapter 4.

In Chapter 4.1, a 9 : 1 binary mixture of $[C_2C_1Im][Tf_2N]$: $[C_{12}C_1Im][Tf_2N]$ is probed by ARXPS. As demonstrated in Chapter 3.1, ILs containing a hydrophobic alkyl chain at the imidazolium cation show an enrichment of this alkyl chain at the outer surface. Furthermore, $[C_{12}C_1Im][Tf_2N]$ exhibits a lower surface tension than $[C_2C_1Im][Tf_2N]$. From both these factors one could expect surface enrichment of $[C_{12}C_1Im]^+$ at expense of $[C_2C_1Im]^+$. However, ARXP spectra of the binary mixture show a homogeneous distribution of the cations, indicating the complexity of enrichment effects.

The surface activity of the cationic head group is probed in Chapter 4.2. While the equimolar mixture of $[S(CH_3)_3][Tf_2N]$: $[C_2C_1Im][Tf_2N]$ exhibits a homogeneous distribution of the ions, a slight surface enrichment of $[P_{4441}]^+$ at expense of $[C_8C_1Im]^+$ is observed in the equimolar mixture of $[P_{4441}][MeOSO_3]$ and $[C_8C_1Im][MeOSO_3]$.

In Chapter 4.3, it is shown that perfluoroalkyl compounds not only exhibit a high surface activity in aqueous solutions[28, 29], but also in IL systems. Hereto, the ARXPS results of a 1 : 1 mixture of $[C_2C_1Im]I$ and $[C_2C_1Im][Pf_2N]$ are presented.

The surface compositions of IL solutions are discussed in Chapter 4.4. In particular, the effect of the ligands on the surface activity of a Rh^I complex is addressed. While $[Rh(acac)(CO)_2]$ shows no surface enrichment in $[C_2C_1Im][EtOSO_3]$, exchanging one CO ligand by a tppts ligand leads to the surface segregation of the catalytic-active Rh^I complex.

In Chapter 5, it is shown that the use of *in situ* XPS for the monitoring of liquid-phase reactions is principally possible and might also be adapted in the future to study SILP reactions. The advantage of *in situ* XPS, as compared to common analytical methods, such as NMR, is that all elements (apart from hydrogen and helium) can be quantified and analysed with respect to their chemical state (*e.g.*, oxidation state) within one experiment. We are even able to follow an organic reaction with *in situ* XPS, when the reacting groups have been linked before-hand to an ionic head group to drastically lower the vapour pressures of the reactants. The studied reaction involves the alkylation of an amine by a chloroalkyl species (Chapter 5.1). In the course of the reaction, the covalently bound chlorine is converted to chloride and the amine to ammonium as reflected by distinct shifts in the N 1s and Cl 2p binding energies.

The irradiation with high energetic X-rays can also trigger reactions. Chapter 5.2 addresses the X-ray induced reduction of the Pt^{IV} complex $[PtCl_6]^{2-}$ dissolved in IL. The dependence of this reduction on the IL anion is probed by using $[C_2C_1Im][EtOSO_3]$ and $[C_2C_1Im][Tf_2N]$ as solvents. While with $[C_2C_1Im][EtOSO_3]$ a complete reduction of Pt^{IV} to

Pt^{II} is observed upon prolonged X-ray irradiation, with $[C_2C_1Im][Tf_2N]$ only a partial reduction occurs.

The gas/IL interaction is not only important for the SILP process, but also for possible applications of ILs as gas storage and gas separation media.[30, 31] For this purpose the interaction of NH_3 with the IL $[C_8C_1Im][CuCl_3]$ is probed with *in situ* XPS (Chapter 5.3). By cooling the IL to ~229 K and dosing NH_3, a signal for an absorbed NH_3 species is observed in the N 1s region. Simultaneous changes in the satellite structure of the Cu $2p_{3/2}$ signal suggest the chemisorption of NH_3.

This work serves as a milestone to the understanding of IL surfaces in general and also to the interface processes in the SILP catalysis in particular. While for the solid/IL interface the PhD thesis of Till Cremer[32] is recommended, this work concentrates on the vacuum/IL (gas/IL) interface. By presenting a combination of already published and unpublished data, an overview of the surface properties of neat ILs, IL mixtures and IL solutions is given in this thesis. Furthermore, the suitability of *in situ* XPS for reaction monitoring is proven.

2. Fundamentals and Techniques

2.1. X-ray photoelectron spectroscopy

In this chapter only the basic aspects of X-ray photoelectron spectroscopy (XPS) will be presented; for further details the book of Hüfner[23] and the book of Briggs and Seah[33] are recommended.

Photoelectron spectroscopy is based on the photoelectric effect: The irradiation of a sample with photons of defined energy $h\nu$ larger than the ionisation energy leads to the emission of electrons. As high energetic X-rays with $h\nu > 100$ eV are used for XPS, electrons from core levels can be excited above the vacuum level. To probe valence states, the closely related ultra-violet photoelectron spectroscopy (UPS) is used with photon energies lower than 100 eV.

The kinetic energy (E_{kin}) of the emitted photoelectrons is usually measured with a hemispherical electron analyser. Taking the work function of the analyser (Φ_{an}) into account, the binding energy (E_B) of the electrons in matter can be derived by the equation

$$E_B = h\nu - E_{kin} - \Phi_{an}. \qquad (1)$$

Each element has a characteristic set of XP signals, enabling a qualitative analysis of the sample. But also the quantitative analysis of the chemical composition of the sample is possible as the signal intensities are proportional to the number of atoms. Furthermore, the binding energies of the core electrons exhibit a chemical shift, which is caused by the chemical state of the atom, enabling *inter alia* the differentiation between oxidation states.

The surface sensitivity of XPS is caused by the low inelastic mean free path of electrons (λ_e) in matter, whereby λ_e is dependent on the kinetic energy of the electrons. As an Al-K_α X-ray source ($h\nu = 1486.6$ eV) is utilised in this work, the photoelectrons (of the elements studied here) possess kinetic energies in the range of 500 - 1400 eV and, therefore, a λ_e of about 1 - 1.5 nm in inorganic solids.[34] However, organic systems, like polymers and the herein studied ILs, exhibit a lower mass density, which results in an about two to three times larger λ_e than in inorganic solids.[35] The effective information depth (ID) of XPS is given by the equation

$$ID = 3\lambda_e \cdot \cos\vartheta, \qquad (2)$$

where ϑ is the emission angle (angle between the surface normal of the sample and the analyser). With increasing emission angle the information depth decreases. This correlation is exploited in angle-resolved XPS (ARXPS): A preferential increase in the core level intensity with increasing emission angle and, thus, with increasing surface sensitivity indicates a higher concentration of this element in the topmost layers as compared to the 0° emission. Therefore, statements about surface orientation and enrichment effects are possible.

2.2. Experimental details

Materials and Sample Preparation. The ILs used in this work are summarised in Table 2.2 with their respective abbreviation, structure and IUPAC name. Additionally, the origins of the ILs are listed in Table 2.2. Most of the ILs were synthesised and characterised in the group of Prof. Peter Wasserscheid at the "Lehrstuhl für Chemische Reaktionstechnik". All synthesised ILs were dried after preparation in vacuum ($9 \cdot 10^{-3}$ mbar) at 40 °C for 24 h. The purities of the samples were verified by ^{1}H NMR analysis (JEOL, ECX +400 spectrometer), with dimethyl sulfoxide-d_6 (DMSO-d_6) as solvent. The total peak integral in the ^{1}H NMR spectrum was found to correspond for all ILs to a nominal purity higher than 99%, apart from $[C_{10}C_1Im][Tf_2N]$, where a purity of higher than 98% was found, and $[(CF_3(CF_2)_3(CH_2)_2)$-$C_1Im]I$ where residual signals of the starting material were observed.

$[C_8C_1Im]I$ was synthesised in the group of Dr. Pete Licence of the University of Nottingham and $[C_8C_1Im][NO_3]$ in the group of Prof. Stefan Spange of the University of Chemnitz; both ILs had a purity of >99%. $[P_{4441}][MeOSO_3]$ was kindly provided to us by Iolitec (www.iolitec.de, purity >95%) and $[C_8C_1Im][B(CN)_4]$ and $[C_8C_1Im][FAP]$ by Merck (purity >99%). $[C_2C_1Im][BF_4]$ and $[C_8C_1Im]Br$ were purchased from Merck with a purity of >98%. $[C_8C_1Im][BF_4]$, $[C_8C_1Im][PF_6]$, and $[C_8C_1Im][TfO]$ were purchased from Sigma-Aldrich with a purity of >97%, > 95%, and >97%, respectively. $[Rh(acac)(CO)_2]$ and Na_3tppts were purchased from Strem Chemicals, and NH_3 (purity 3.8) was purchased from Linde.

The preparation of the saturated metal complex solutions in ILs was done in the group of Prof. Wasserscheid. The metal compound was added to the relevant ionic liquid (~2.0 g) in the amount necessary to get a 0.1 mol/mol solution. Acetonitrile was added as a co-solvent to enhance the solubility of the complex. The resulting suspension was stirred at room temperature for ~24 h. After evaporation of the co-solvent and centrifugation, in order to remove the un-dissolved material, the supernatant fluid was separated and analysed for the metal content by means of inductively-coupled plasma atomic emission spectroscopy (ICP-

AES). The binary IL mixtures were also prepared with acetonitrile as co-solvent to ensure a homogeneous distribution of the ions.

The thin IL films (thickness: 50 - 100 µm) were prepared by deposition of the corresponding IL onto a planar Au foil (20 mm × 15 mm × 0.1 mm). These samples were then introduced into the UHV system via a load lock where residual co-solvents and volatile contaminations like water evaporated.

UHV apparatus. The XPS setup used for the measurements presented in this thesis is based on the "ESCALAB 200 spectrometer" (Vacuum Generators LTD), which originally consists of a load lock and an analysis chamber and was upgraded by a preparation chamber; a detailed description of the chambers can be found in the PhD theses of M. Probst[36] and F. Grellner[37].

The samples are introduced in the apparatus via the load lock, where a base pressure of ~$1 \cdot 10^{-6}$ mbar is reached. The preparation chamber is equipped with a sputter gun for sample cleaning by Ar^+ bombardment, a quartz-crystal microbalance (QCM), and an evaporator for organic material. Furthermore, the possibility to dose gases and to measure LEED (Low Energy Electron Diffraction) is given in the preparation chamber. An Al/Mg-dual X-ray gun, an UV lamp, an electron gun, and a concentric hemispherical electron energy analyser (CHA) are mounted at the analysis chamber, which enables the measurement of XPS, UPS and AES (Auger Electron Spectroscopy). The analysis chamber is also equipped with a quadrupole mass spectrometer (QMS). The base pressure in the preparation and analysis chamber is below $1 \cdot 10^{-9}$ mbar. The pressure in the UHV apparatus is maintained by two ion getter pumps, two titan sublimation pumps, four turbomolecular pumps, and six rotary vane pumps.

For the *in situ* preparation and the XPS measurements the sample is mounted on the head of a manipulator, which is manoeuvrable in *x*-, *y*-, and *z*-direction and can be rotated around its *z*-axis, enabling the measurement of ARXPS. Furthermore, the manipulator allows for the cooling of the sample to ~90 K with liquid nitrogen. The manipulator head was upgraded during the course of this thesis; detailed descriptions of the old and the new manipulator head can be found in the PhD theses of M. Probst[36] and T. Cremer[32], respectively. With both designs the sample can be heated to at least ~1200 K by means of an electron beam heating. However, with the new design the attachment of a thermocouple near the sample is possible, resulting in a lower error of ± 5 K for the temperature reading. With the old design, the thermocouple was only attached to the side of the manipulator head, which led to an unreliable temperature reading.

During the duration of the PhD thesis also the energy analyser and the X-ray gun of the "ESCALAB 200 spectrometer" were replaced by the "VG Scienta R3000" analyser and the "SPECS XR50" X-ray gun; the latter is also an Al/Mg-dual X-ray gun, but features an additional water-cooling system to minimise the heat transfer from the X-ray anode to the sample. The characterisation of the new analyser can be found in ref. [38].

Data acquisition. Non-monochromatised Al-K_α radiation ($h\nu$ = 1486.6 eV) was used for the measurement of the XP spectra. As X-ray source served either the "SPECS XR50" X-ray gun at a power of 250 W (U = 12.5 kV, I = 20 mA) or the X-ray gun of the "VG ESCALAB 200" at a power of 150 W (U = 15 kV, I = 10 mA). The latter X-ray gun was positioned at a smaller distance to the sample. Overall the intensity of the "VG ESCALAB 200" X-ray gun was 9% smaller than for the "SPECS XR50" X-ray source.

The CHA of the "ESCALAB 200" was operated with pass energies of 100 and 20 eV for survey scans and core level spectra, respectively. For the "VG Scienta R3000" analyser, pass energies of 200 eV for survey scans and 100 eV for core level spectra were chosen.

Table 2.2 lists which setup was used for the individual ILs: ① presents the original "ESCALAB 200" system, ② stands for the new CHA combined with the old X-ray gun, and ③ implies the combination of the new CHA and the new X-ray gun.

To vary the surface sensitivity of the measurements, spectra were collected under 0° and 80° emission. Considering the inelastic mean free path of ~2 - 3 nm of photoelectrons in organic compounds at the kinetic energies used (~500 - 1400 eV)[35], measurements at 0° probe the near-surface region (*ID* = 7 - 9 nm) and at 80° (*ID* = 1 - 1.5 nm) probe the topmost layers. (Note: To correct for reduced overall transmission at 80° emission, the corresponding spectra were multiplied by an empirical factor.)

Data analysis. For most of the studied core level spectra a two-point linear background was subtracted; the only exceptions were the C 1s spectra of the systems containing the $[Tf_2N]^-$ anion and the Cu $2p_{3/2}$ spectra, where a three-point linear background subtraction was applied. The data obtained with the original "VG ESCALAB 200" setup were evaluated with the "Origin 7.5 SR6" software, where Gauss-functions were used for fitting the spectra. With the "VG Scienta R3000" analyser the "CasaXPS" software (version 2.3.16Dev6) was used for data evaluation and enabled the fitting with a Gauss-Lorentzian profile with 30% Lorentz contribution (note that the use of different line shapes did not significantly influence the quantitative results reported in this work).

XP signals of p, d and f orbitals are split into two peaks due to spin-orbit coupling. The binding energy separation of the two peaks is individual for each core level (see Table 2.1), while the intensity ratio of the two peaks always equals 2 : 1 for $p_{3/2} : p_{1/2}$, 3 : 2 for $d_{5/2} : d_{7/2}$, and 4 : 3 for $f_{7/2} : f_{5/2}$.[23]

By analysis of the peak areas and by considering the sensitivity factors for the different elements, quantitative information on the overall stoichiometry of the investigated sample can be derived from the spectra. The atomic sensitivity factors (ASFs) used, were calibrated for our specific experimental setup to account for the transmission function of the analyser. For the calibration, two ultraclean and well-characterised ILs, namely, $[C_2C_1Im][Tf_2N]$ and $[C_2C_1Im][EtOSO_3]$, were measured in normal emission as reference. Due to the small molecular volume of the ILs compared to the inelastic mean free path of electrons, surface orientation effects are negligible. By considering the nominal atom ratios of the ILs, the ASF values for C 1s, N 1s, O 1s, and S 2p – referenced to ASF (F 1s) = 1 – were derived from the area analysis of the XP signals in 0° emission.

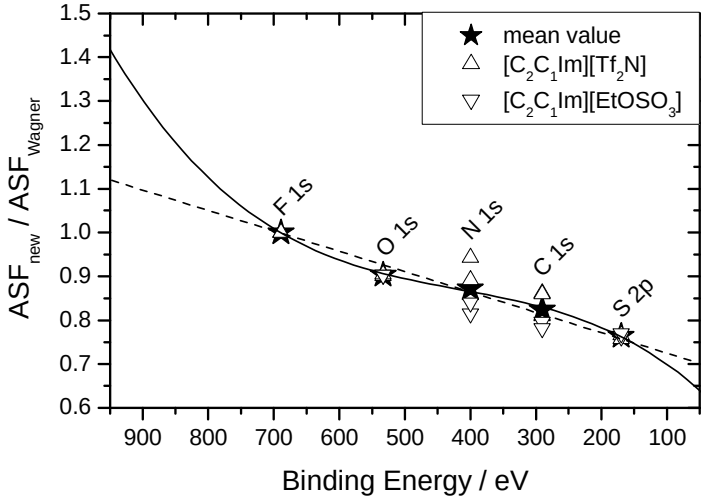

Figure 2.1. Dependence of the ratio of the calculated ASF values for the "VG Scienta R3000" analyser (ASF_{new}) *vs.* the ASF values of Wagner (ASF_{Wagner})[39] on the binding energy.

The dependence of the ratio of the calculated ASF values *vs.* the ASF values of Wagner[39] on the binding energy is shown in Figure 2.1 for the "VG Scienta R3000" analyser. By fitting the data with a third degree polynomial, the ASF values for B 1s, Cl 2p, I $3d_{5/2}$, P 2p, and Rh 3d were obtained. This procedure enables only the calculation of ASF values for core levels in the binding energy range of 100 - 800 eV within an accuracy of ± 5% (note that a linear fit yield changes to these values of < 3%). Therefore, the ASF values of core levels in the lower and in the higher binding energy regime were calculated by other ways. For the ASF of Pt 4f, the X-ray stable salts $[Pt(NH_3)_4]Cl_2$ and $K_2[PtCl_4]$ were chosen and the ASF

value was calculated by considering the nominal atom ratio of Pt : N and Pt : Cl, respectively. The ASF of Cu $2p_{3/2}$ was derived by the linear fitting of the data shown in Figure 2.1. The accuracy of the calculated ASF values is in both cases about ± 10%. All calculated ASF values for the "VG ESCALAB 200" setup (ASF_{old}), the "VG Scienta R3000" analyser (ASF_{new}), and the ASF values of Wagner (ASF_{Wagner}) are listed in Table 2.1.

Table 2.1: Approximate binding energies E_B for the individual core levels, atomic sensitivity factors given by Wagner (ASF_{Wagner}), and calibrated atomic sensitivity factors for the "VG ESCALAB 200" system (ASF_{old}) and the "VG Scienta R3000" analyser (ASF_{new}). In case of p, d and f orbitals, the binding energy separation E_B^{sep} of the doublet is also listed.

XP signal	E_B [eV]	ASF_{Wagner} [a]	ASF_{old}	ASF_{new}	E_B^{sep} [eV]
Pt 4f	75	4.40	3.40	3.60	3.35
P 2p	135	0.39	0.28	0.29	0.97
S 2p	170	0.54	0.40	0.41	1.18
B 1s	188	0.13	0.10	0.10	-
Cl 2p	200	0.73	0.56	0.55	1.6
C 1s	287	0.250	0.205	0.210	-
Rh 3d	310	4.10	3.36	3.44	4.75
N 1s	400	0.42	0.35	0.36	-
O 1s	531	0.66	0.58	0.60	-
I $3d_{5/2}$	631	6.00	5.61	5.74	-
F 1s	689	1.00	1.00	1.00	-
Cu $2p_{3/2}$	933	4.20	-	4.60	-

[a] ref. [39]

Table 2.2: Summary of studied ILs.

Abbreviation	Structure	IUPAC name	Origin	XPS setup[a]	Chapter
$[C_nC_1Im][Tf_2N]$ (n = 1, 2, 4, 6, 8, 10, 12, 16)	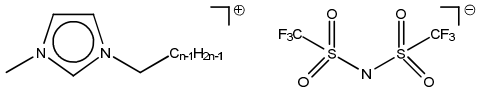	1-alkyl-3-methylimidazolium bis[(trifluoromethyl)sulfonyl]imide	Natalia Paape Prof. Wasserscheid	①	3.1, 3.2, 4.1, 4.2, 5.2
$[C_2C_1Im]I$	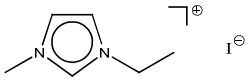	1-ethyl-3-methylimidazolium iodide	Natalia Paape Prof. Wasserscheid	①	4.3
$[C_2C_1Im][BF_4]$	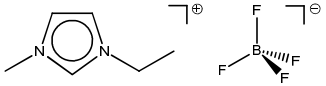	1-ethyl-3-methylimidazolium tetrafluoroborate	Merck	①	3.2
$[C_2C_1Im][EtOSO_3]$	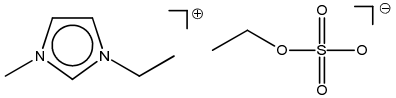	1-ethyl-3-methylimidazolium ethylsulfate	Natalia Paape Prof. Wasserscheid	①	4.4, 5.2
$[C_2C_1Im][Pf_2N]$	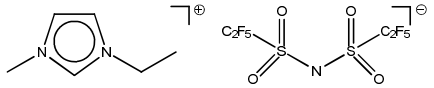	1-ethyl-3-methylimidazolium bis[(pentafluoroethyl)sulfonyl]imide	Natalia Paape Prof. Wasserscheid	①	4.3
$[C_2C_1Im]$ $[ClC_4H_8SO_3]$	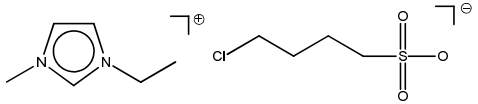	1-ethyl-3-methylimidazolium 4-chlorobutylsulfonate	Nicola Taccardi Prof. Wasserscheid	③	3.3, 5.1
$[C_2C_1Im]_2[PtCl_6]$	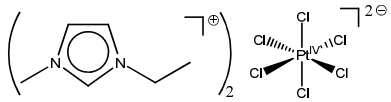	1-ethyl-3-methylimidazolium hexachloroplatinate(IV)	Natalia Paape Prof. Wasserscheid	①	5.2
$[C_8C_1Im]Cl$	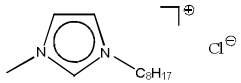	1-methyl-3-octylimidazolium chloride	Natalia Paape Prof. Wasserscheid	①	3.2
$[C_8C_1Im]Br$	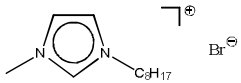	1-methyl-3-octylimidazolium bromide	Merck	①	3.2

Table 2.2 continued.

Abbreviation	Structure	IUPAC name	Origin	XPS setup[a]	Chapter
$[C_8C_1Im]I$	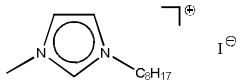	1-methyl-3-octylimidazolium iodide	Dr. P. Licence (University of Nottingham)	①	3.2
$[C_8C_1Im][NO_3]$	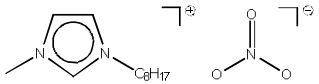	1-methyl-3-octylimidazolium nitrate	Prof. S. Spange (University of Chemnitz)	①	3.2
$[C_8C_1Im][BF_4]$	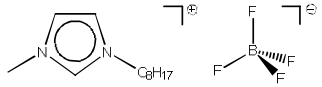	1-methyl-3-octylimidazolium tetrafluoroborate	Sigma-Aldrich	①	3.2
$[C_8C_1Im][PF_6]$	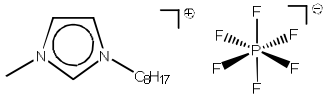	1-methyl-3-octylimidazolium hexafluorophosphate	Sigma-Aldrich	①	3.2
$[C_8C_1Im][B(CN)_4]$	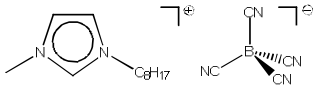	1-methyl-3-octylimidazolium tetracyanoborate	Merck	①	3.2
$[C_8C_1Im][MeOSO_3]$	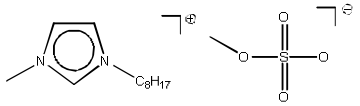	1-metyl-3-octylimidazolium methylsulfate	Natalia Paape Prof. Wasserscheid	①	3.2, 4.2
$[C_8C_1Im][TfO]$	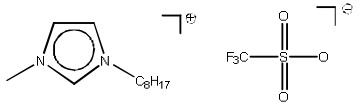	1-methyl-3-octylimidazolium trifluoromethylsulfonate	Sigma-Aldrich	①	3.2
$[C_8C_1Im][Pf_2N]$	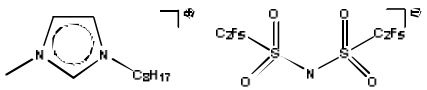	1-methyl-3-octylimidazolium bis[(pentafluoroethyl)sulfonyl]imide	Natalia Paape Prof. Wasserscheid	①	3.2
$[C_8C_1Im][FAP]$	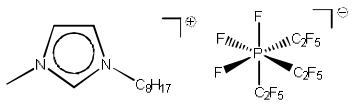	1-methyl-3-octylimidazolium tris(pentafluoroethyl)trifluorophosphate	Merck	①	3.2

Table 2.2 continued.

Abbreviation	Structure	IUPAC name	Origin	XPS setup[a]	Chapter
$[C_8C_1Im]$ $[ClC_4H_8SO_3]$	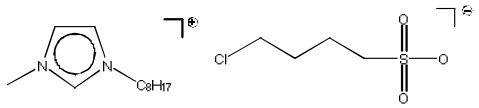	1-methyl-3-octylimidazolium 4-chlorobutylsulfonate	Nicola Taccardi Prof. Wasserscheid	②	5.1
$[C_8C_1Im][CuCl_3]$	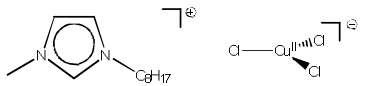	1-methyl-3-octylimidazolium trichlorocuprate(II)	Daniel Roth Prof. Wasserscheid	③	5.3
$[(CF_3(CF_2)_3$-$(CH_2)_2)C_1Im]I$	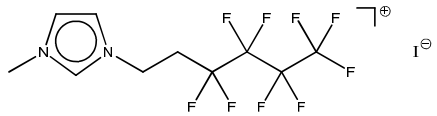	1-methyl-3-(3´,3´,4´,4´,5´,5´,6´,6´,6´-nonafluorohexyl)imidazolium iodide	Wei Wei Prof. Wasserscheid	①	3.3
$[(Me_2NC_3H_4)C_1Im]$ $[TfO]$	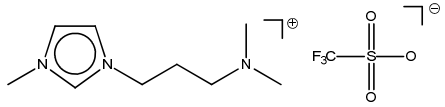	1-methyl-3-(3`-dimethylaminopropyl)-imidazolium trifluoromethylsulfonate	Nicola Taccardi Prof. Wasserscheid	③	3.3, 5.1
$[(Me_2NC_3H_4)C_1Im]$ $[Tf_2N]$	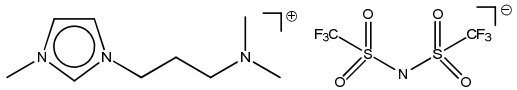	1-methyl-3-(3`-dimethylaminopropyl)-imidazolium bis[(trifluoromethyl)sulfonyl]imide	Nicola Taccardi Prof. Wasserscheid	②	3.3, 5.1
$[Me(EG)_2C_1Im]$ $[Tf_2N]$	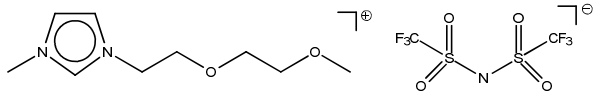	1-[2-(2-methoxy-ethoxy)ethyl]-3-methylimidazolium bis[(trifluoromethyl)sulfonyl]imide	Wei Wei Prof. Wasserscheid	①	3.3
$[S(CH_3)_3][Tf_2N]$	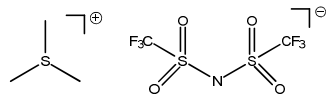	trimethylsulfonium bis[(trifluoromethyl)sulfonyl]imide	Wei Wei Prof. Wasserscheid	①	4.2
$[P_{4441}][MeOSO_3]$	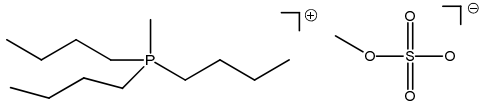	methyl-tributylphosphonium methylsulfate	iolitec	①	4.2

Table 2.2 continued.

Abbreviation	Structure	IUPAC name	Origin	XPS setup[a]	Chapter
$[PBu_4][ClC_4H_8SO_3]$	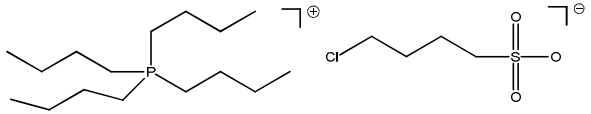	tetrabutylphosphonium 4-chlorobutylsufonate	Nicola Taccardi Prof. Wasserscheid	③	5.1
$[(Me_2NC_3H_4)PBu_3]$ [FAP]	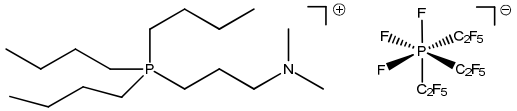	(3`-dimethylaminopropyl)-tributylphosphonium tris(pentafluoroethyl)trifluorophosphate	Nicola Taccardi Prof. Wasserscheid	③	3.3, 5.1
$[Pt(NH_3)_4][Tf_2N]_2$	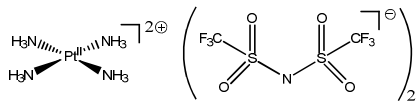	tetraaminoplatinum(II) bis[(trifluoromethyl)sulfonyl]imide	Natalia Paape Prof. Wasserscheid	①	5.2
$[Rh(acac)(CO)_2]$	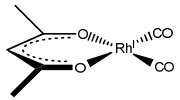	dicarbonylacetylacetonatorhodium(I)	Strem Chemicals	①	4.4
Na_3tppts	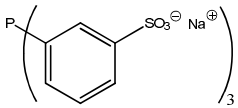	tris(3-sodium sulfonatophenyl) phosphine	Strem Chemicals	①	4.4

[a]① "ESCALAB 200" analyser and X-ray gun
② "VG Scienta R3000" analyser and "ESCALAB 200" X-ray gun
③ "VG Scienta R3000" analyser and "SPECS XR50" X-ray gun

3. Surface ordering and surface tension of neat ionic liquids

In this chapter, a selection of major results on surfaces of neat ILs are presented, which are based on the following publications (see also Appendix) along with unpublished data:

[P1] K. R. J. Lovelock, **C. Kolbeck**, T. Cremer, N. Paape, P. S. Schulz, P. Wasserscheid, F. Maier, H.-P. Steinrück
Influence of Different Substituents on the Surface Composition of Ionic Liquids Studied Using ARXPS
J. Phys. Chem. B 113 (2009) 2854-2864.

[P3] **C. Kolbeck**, J. Lehmann, K. R. J. Lovelock, T. Cremer, N. Paape, P. Wasserscheid, A. P. Fröba, F. Maier, H.-P. Steinrück
Density and Surface Tension of Ionic Liquids
J. Phys. Chem. B 114 (2010) 17025-17036.

[P6] I. Niedermaier, **C. Kolbeck**, N. Taccardi, P. S. Schulz, J. Li, T. Drewello, P. Wasserscheid, H.-P. Steinrück, F. Maier
Organic Reactions in Ionic Liquids Studied by in Situ XPS
ChemPhysChem 13 (2012) 1725-1735.

This thesis focuses on surfaces of ionic liquids, particularly on IL-vacuum interfaces. Insights into thermodynamic properties such as surface tension and surface composition (in equilibrium) also help for a better understanding of everyday life and of industrial surface and interface related applications, like filtration, wetting, lubrication, washing, adsorption, vaporisation, heterogeneous reactions, and many more. Both, surface tension and surface composition are closely related. As already pointed out by Irving Langmuir, surface tension is closely related to the intermolecular interactions in the bulk (cohesive energy) and the molecular orientation at the surface.[40, 41] According to the “principle of independent action between surfaces of molecules”, which is also known as “Langmuir principle”, these intermolecular interactions mainly depend on the nature of those chemical groups of the interacting molecules, which are in contact with each other.[40] To minimise surface energy, molecules very close to the surface preferentially orientate themselves in such a way that chemical groups of the molecules, which are least attracted by neighbouring molecules, preferentially point towards the gas/vacuum side, whereas chemical groups most strongly attracted by their neighbours preferentially point towards the bulk. Within the framework of the “Langmuir principle”, the surface tension is given by the superposition of the contributions from only those chemical groups that form the outer surface.[40] Whereas only

relatively simple laboratory equipment is required for surface tension measurements, the determination of molecular orientation at liquid surfaces is more challenging. Because most surface science methods are restricted to UHV conditions, only a few surface-sensitive methods, like sum frequency generation (SFG)[42-45], X-ray and neutron reflectometry[46-50], and gracing incidence X-ray diffraction[46, 47, 51], as well as computer simulations[46, 47, 52-54] can be applied under ambient conditions to study surface orientation effects in common liquids. The extremely low vapour pressure of ionic liquids[4, 5], however, opens the door to UHV-based surface science methods like X-ray photoelectron spectroscopy (XPS)[55-58], UV photoelectron spectroscopy (UPS)[59-61], inverse photoelectron spectroscopy (IPES)[62-64], X-ray absorption spectroscopy (NEXAFS)[63], metastable ion spectroscopy (MIES)[59, 60], direct recoil spectroscopy (DRS)[20, 21], high resolution electron energy loss spectroscopy (HREELS)[60], low energy ion scattering (LEIS)[65], time-of-flight secondary mass spectroscopy (TOF-SIMS)[66], soft X-ray emission spectroscopy (SXES)[64], neutral impact collision ion scattering spectroscopy (NICISS)[67], and Rutherford backscattering (RBS)[68, 69]. These surface science studies of ILs also open new routes towards the fundamental understanding of the surface properties of liquids in general.

In this chapter, ARXPS was used to obtain information on the mean orientation of the IL ions at the surface. The ARXPS results were correlated with the surface tension and liquid density values of the ILs. The presented surface tension and density data were measured using the pendant drop method and the vibrating tube method, respectively, by Julia Lehmann in the group of Prof. Andreas P. Fröba of the Erlangen Graduate School in Advanced Optical Technologies (SAOT).

In particular, Chapter 3.1 deals with the surface properties of the homologous series of 1-alkyl-3-methylimidazolium bis[(trifluoromethyl)sulfonyl]imide $[C_nC_1Im][Tf_2N]$ (n = 1, 2, 4, 6, 8, 10, 12, 16). The ARXPS results reveal that the $[C_nC_1Im]^+$ cations with $n \geq 4$ are orientated at the surface with the alkyl chains preferentially pointing towards the vacuum, forming an aliphatic overlayer above a polar sublayer, consisting of the imidazolium head groups and the $[Tf_2N]^-$ anions. The thickness of this aliphatic overlayer increases with increasing alkyl chain length, resulting in a lowering of the surface tension.

The influence of the anion on the surface tension is probed by studying 12 ILs with 1-methyl-3-octylimidazolium $[C_8C_1Im]^+$ as cation and a series of anions, which cover different sizes, shapes and coordination abilities (see Chapter 3.2). Here, anions with akin chemical structures are comprised in sub-groups (*e.g.*, halides), and trends of surface tension values are

considered within these groups. In all cases, surface tension values are discussed in terms of surface orientation effects and intermolecular interaction energies.

The implementation of functional groups in the chemical structure of the IL cation or anion and its impact on the orientation of the IL ions at the surface and on the interaction of neighbouring molecules will be discussed in Chapter 3.3. The used functional groups range from weakly interacting perfluoroalkyls to ethylene glycol groups, which have the ability for H-bonding.

3.1. Influence of alkyl chain length[P1, P3]

Using the homologous series of 1-alkyl-3-methylimidazolium bis[(trifluoromethyl)sulfonyl]-imide [C_nC_1Im][Tf_2N] (n = 1, 2, 4, 6, 8, 10, 12, 16), the dependence of the IL surface composition and surface tension on the alkyl chain length will be discussed in the following. Figure 3.1 shows, next to the chemical structure of [C_nC_1Im][Tf_2N], the corresponding C 1s spectra in 0° emission. With n = 1 two different C 1s signals are distinguishable at 292.7 and 286.6 eV, which can be attributed to the trifluoromethyl-groups of the anion (labelled C_{Tf2N}) and to the carbon atoms of the $[C_1C_1Im]^+$ cation (labelled C_{hetero}). With $n \geq 2$ a third signal at lower binding energies (~ 284.8 eV) can be observed, which stems from the carbon atoms solely bound to carbon and to hydrogen (labelled C_{alkyl}). With increasing alkyl chain length, the C_{alkyl} signal increases in intensity, as expected. Concomitantly, both, the C_{hetero} as well as the C_{Tf2N} signal loose intensity with increasing chain length, which is due to the increasing molecular volume V_m of the cation and, thus, the decreasing density of C_{Tf2N} and C_{hetero} atoms.

The orientation of the ions at the surface was probed by ARXPS. As a case study, the C 1s spectra of [C_8C_1Im][Tf_2N] in 0° (black) and 80° emission (gray) are depicted in Figure 3.2a. Changing the detection geometry from 0° to 80° emission, an increase in C_{alkyl} intensity is observed. Because of the very high surface sensitivity at 80°, this increase unambiguously indicates the preferential orientation of the octylchain towards the vacuum. Moreover, damping of all other IL signals occurs, as demonstrated in Figure 3.2a, by the decrease in C_{hetero} and C_{Tf2N} signal intensity. The quantitative analysis reveals that the XP signals of the imidazolium head group are slightly more damped than the anion signal, which indicates a slightly shorter mean distance of the anions to the outer surface compared to the imidazolium ring.

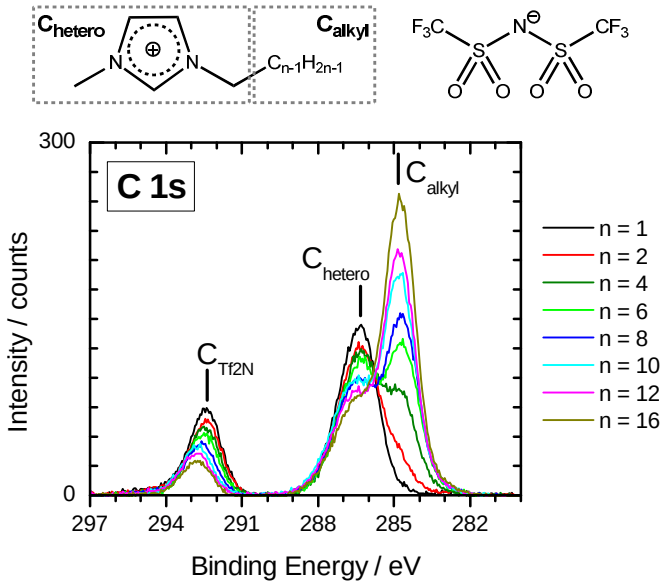

Figure 3.1. Chemical structure and C 1s spectra in 0° emission of $[C_nC_1Im][Tf_2N]$ (n = 1, 2, 4, 6, 8, 10, 12, 16).

Based on these first observations, ARXPS clearly reveals a surface layer of preferentially oriented molecules with an aliphatic overlayer comprised of the alkyl chains, which lies above a polar sublayer, consisting of the imidazolium head groups and the anions.

For a quantitative comparison of the $[C_nC_1Im][Tf_2N]$ systems, the excess of alkyl carbon measured under 80° is evaluated. For this purpose, the ratio

$$R = \frac{I_{C1s}(C_{alkyl};80°)/I_{C1s}(C_{hetero};80°)}{C_{alkyl}(nom.)/C_{hetero}(nom.)}, \qquad (3)$$

where $I_{C1s}(C_{alkyl};80°)$ and $I_{C1s}(C_{hetero};80°)$ are defined as the respective C 1s signal intensities obtained at 80° emission, and $C_{alkyl}(nom.)$ and $C_{hetero}(nom.)$ as the nominal atom ratios, is drawn as a function of alkyl chain length (see Figure 3.2b). While a value of R = 1 indicates an isotropic orientation of the cations, values larger than 1 are a sign of surface enrichment of the C_{alkyl} species at the outer surface; for larger R values the enrichment is more pronounced. Inspection of Figure 3.2b shows that only for $[C_2C_1Im][Tf_2N]$, a ratio of 0.95 ± 0.10 is found, which equals the nominal value in the margin of error and indicates an isotropic arrangement of the $[C_2C_1Im]^+$ cation at the outer surface. Starting at a chain length of $n \geq 4$, an increase in R to values above 1 is observed, suggesting a preferential orientation of the alkyl chain towards the vacuum. The monotone increase in R, when going from n = 4 to 16, clearly indicates an increase in effective thickness of the aliphatic overlayer with increasing n; this is accompanied by a more pronounced damping of the C_{hetero} signal for the longer alkyl chains.

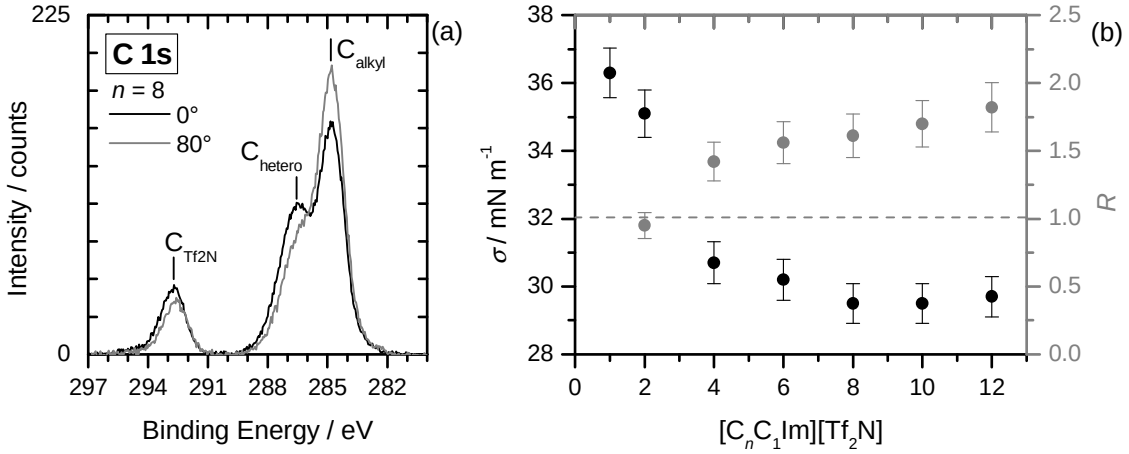

Figure 3.2. a) C 1s spectra of $[C_8C_1Im][Tf_2N]$ in 0° (black) and 80° (gray) emission and b) surface tension σ and ratio R (see equation 3) in dependence of the alkyl chain length of $[C_nC_1Im][Tf_2N]$.

In Figure 3.2b also the surface tension σ values at 298.15 K for the $[C_nC_1Im][Tf_2N]$ ILs with $1 \leq n \leq 12$ are depicted. Starting with $\sigma = 36.3 \pm 0.7$ mN m^{-1} for $[C_1C_1Im][Tf_2N]$, a decrease in surface tension is observed upon increasing the alkyl chain length up to $n = 8$. The most pronounced decrease in surface tension is observed between $n = 1$ and 4. For $n \geq 8$ no further changes in surface tension are observed in the margin of error. This is in agreement with a multiscale coarse-grained molecular dynamic simulation of Jiang *et al.*, predicting a constant surface tension value for $n \geq 10$.[52] Note that since the publication of the paper [P3], Tariq *et al.* also systematically studied the surface tension of $[C_nC_1Im][Tf_2N]$ ILs with $2 \leq n \leq 14$ by means of the pendant drop method; in contrast to our results, they observed a further decrease in surface tension between $n = 12$ to 14 together with some irregular trends in surface tension values ascribed to either changes in bulk structure, surface restructuring, or an influence of possible surface contaminations.[70]

In contrast to the IL series investigated here, the surface tension within homologous series of alkanes and alcohols always increases with increasing alkyl chain length, which is explained by an increasing contribution of van-der-Waals energies.[71] Also in the $[C_nC_1Im][Tf_2N]$ series, a longer alkyl chain results in an increased van-der-Waals energy as was shown by a molecular dynamics simulation of Ludwig *et al.*[72] The authors also showed that the Coulomb interactions are only slightly influenced by the alkyl chain length for $n \geq 2$; only for $[C_1C_1Im][Tf_2N]$ a slightly higher Coulomb energy can be observed due to the symmetry of the cation.[72] In the case of a bulk truncated surface, an overall increase of attractive interactions (mainly by the increase in van-der-Waals energies) should thus result in

increasing surface tension values. However, as demonstrated by the ARXPS analysis discussed above, the alkyl chains of the here studied ILs tend to point towards the vacuum/gas phase, forming an aliphatic overlayer above the subjacent imidazolium rings and the anions. Therefore, only a fraction of the Coulomb energy will contribute to the surface tension. With increasing alkyl chain length the aliphatic overlayer will increase and the contribution of the Coulomb energy to the surface tension decrease, resulting in a lower surface tension. When $n \geq 8$ the decrease in Coulomb contribution is probably balanced by the increase in van-der-Waals energy, resulting in the more or less observed constant surface tension.

3.2. Influence of the anion[P3]

The dependence of the surface tension on the anion was probed by measuring 12 different $[C_8C_1Im]^+$-based ILs, with different anions, which cover increasing sizes (from small Cl^- to large $[FAP]^-$), different coordination abilities (from strongly coordinating halides to weakly coordinating anions with fluoroalkyl-groups) and different shapes (from spherical to elongated anions). The chemical structures of the respective anions are depicted in Scheme 3.1 with their abbreviation and IUPAC name.

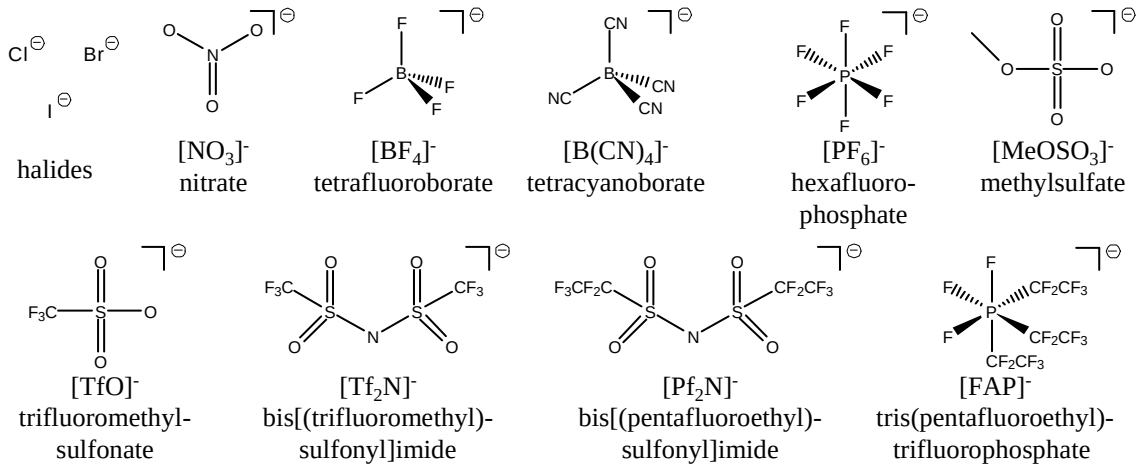

Scheme 3.1. Summary of all investigated anions.

A detailed ARXPS study on the surface compositions of all $[C_8C_1Im]^+$ based ILs can be found in the PhD thesis of Till Cremer.[32] A short overview of the results is given in Figure 3.3b where the XPS intensity ratio of C_{alkyl} / C_{hetero} measured in 80° emission is drawn as a function of molecular volume V_m. For all ILs, a positive deviation from the nominal value (dashed line in Figure 3.3b) is found, indicating that the octyl chain preferentially orientates

itself towards the vacuum in all cases. However, the deviation is stronger for smaller anions than for larger anions. Due to a smaller molecular volume of the anion, the distance between neighbouring octyl chains is smaller, resulting in a stronger van-der-Waals interaction between the chains and, most likely, in a stronger preferential orientation of alkyl chains towards the vacuum accompanied by a stronger damping of core levels of the charged IL moieties. An exception forms $[C_8C_1Im][B(CN)_4]$, which exhibits the overall lowest C_{alkyl} / C_{hetero} ratio (*i.e.*, a weak preferential orientation at the surface) for this medium sized IL.

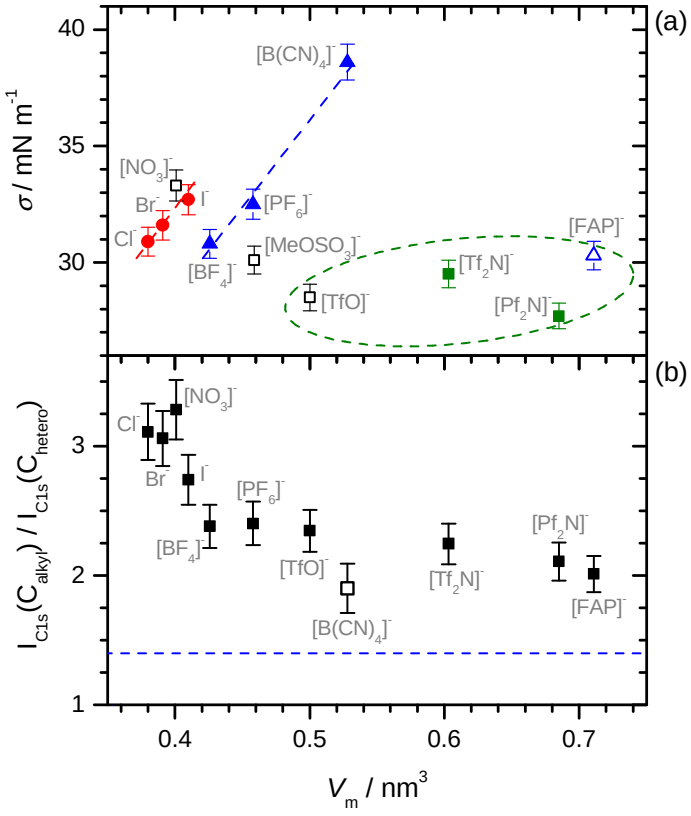

Figure 3.3. a) Surface tension σ of $[C_8C_1Im]^+$ salts at 298.15 K as a function of molecular volume V_m. (Dashed lines indicate trends in subgroups.) b) C_{alkyl} *vs*. C_{hetero} ratio of XPS peak intensities of $[C_8C_1Im]^+$ salts measured in 80° emission as a function of V_m. (Dashed line indicates nominal values for C_{alkyl} *vs*. C_{hetero} as expected from IL stoichiometry.)

Figure 3.3a shows the surface tension σ of all $[C_8C_1Im]^+$ based ILs at 298.15 K as a function of molecular volume V_m. The highest surface tension is found for $[C_8C_1Im][B(CN)_4]$ (38.6 ± 0.8 mN m^{-1}). In contrast, all other $[C_8C_1Im]^+$ based ILs exhibit surface tensions in the range of 27.7 - 33.3 mN m^{-1}. This small range in surface tension is most likely caused by the above mentioned orientation and surface domination of the octyl chains, resulting in only minor contributions of the Coulomb energy to the surface tension. Comparison of the surface tensions of $[C_2C_1Im][Tf_2N]$ (53.9 ± 1.1 mN m^{-1}) and $[C_2C_1Im][BF_4]$ (35.1 ± 0.7 mN m^{-1}),

which differ from each other by 18.8 mN m^{-1}, with the surface tension values of $[C_8C_1Im][Tf_2N]$ (30.8 ± 0.6 mN m^{-1}) and $[C_8C_1Im][BF_4]$ (29.5 ± 0.6 mN m^{-1}), where only a variation of 1.3 mN m^{-1} is found, emphasises the effect of the oriented octyl chains.

In contrast to the obvious dependence of the surface tension on the alkyl chain length (see Chapter 3.1), no general dependence on the molecular volume of the anion can be observed. This is attributed to the fact that there are several factors influencing the interaction forces and, therefore, the surface tension: An increased molecular volume of the anion results in a lower Coulomb interaction, as the mean distance between anions and cations increases, and in a lower contribution of the van-der-Waals energies of the alkyl chains, as the density is decreased. Thus, the surface tension is expected to be lower for bigger anions. A contrary effect that would lead to an increase in surface tension is most likely responsible for the observed trend seen within the halide series (red dashed line in Figure 3.3a) and within the series of medium-sized spherical anions $[BF_4]^-$, $[PF_6]^-$ and $[B(CN)_4]^-$ (blue dashed line in Figure 3.3a). In both cases, an increase in surface tension is observed with increasing molecular volume, which is likely to be related to an increasing polarisability and, therefore, an increasing van-der-Waals contribution of the anions.[73-76]

Finally, low surface tensions (27.7 - 30.3 mN m^{-1}) are found for anions containing perfluoroalkyl-groups, namely $[TfO]^-$, $[Tf_2N]^-$, $[Pf_2N]^-$, and $[FAP]^-$ (see dashed ellipse in Figure 3.3a). Comparison with common non-ionic molecular liquids shows that the perfluorination of alkanes generally results in lower surface tension due to the very rigid and non-coordinating C-F bonds, leading to only very weak attractive interactions between the CF_x groups (in contrast to the polarisable C-H bonds in the case of hydrocarbons); moreover, steric repulsion effects between CF_x groups are also proposed to be involved in lowering the surface tension.[77]

3.3. Functionalised ionic liquids

In this section, the surface composition of functionalised ILs will be discussed. The functional groups implemented in the IL structure are perfluoroalkyl, chloroalkyl, tertiary amine and ethylene glycol; the respective ions are depicted in Scheme 3.2. These functional groups exhibit different intermolecular forces. While C-F bonds exhibit weak attractive interactions[77], C-Cl bonds have a greater polarisability and, therefore, more-attractive van-der-Waals potential.[78] In fact, chloroalkanes exhibit stronger intermolecular interactions than the analogous alkanes, as can be comprehended by comparison of their melting points.[71] Next to

van-der-Waals interactions, amines and ether groups have also the ability to form H-bonds. Apart from the general influence of functional groups on attractive interactions to neighbouring molecules, functional groups could directly influence the orientation of the IL ions at the surface, as they will orientate themselves in such a way that the part, which exhibits the lowest attractive interaction, will point towards the gas phase to minimise the surface tension.

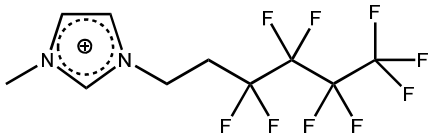

$[(CF_3(CF_2)_3(CH_2)_2)C_1Im]^+$
1-methyl-3-(3´,3´,4´,4´,5´,5´,6´,6´,6´-nonafluorohexyl)imidazolium

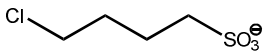

$[ClC_4H_8SO_3]^-$
4-chlorobutylsulfonate

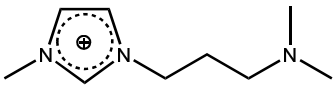

$[(Me_2NC_3H_6)C_1Im]^+$
1-methyl-3-(3'-dimethyl-aminopropyl)imidazolium

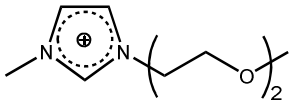

$[(Me(EG)_2C_1Im]^+$
3-[2-(2-methoxy-ethoxy)-ethyl]-1-methylimidazolium

Scheme 3.2. Summary of functionalised IL compounds (either in the cation or in the anion)

Perfluoroalkyl-functionalised ILs. Measured initially at room temperature, the XP spectra of the perfluorinated IL $[(CF_3(CF_2)_3(CH_2)_2)C_1Im]I$ display a shift of the signals of ~5 eV towards higher binding energies, indicating charging of the sample during X-ray irradiation. Furthermore, next to the main I $3d_{5/2}$ signal, which can be attributed to a iodide species, a second smaller signal is observed ~2.5 eV towards higher binding energy, suggesting the presence of covalent iodine, which probably stems from the starting material 1-iodo-1H,1H,2H,2H-perfluorohexane used in the IL synthesis. To overcome sample charging, the sample was first heated in vacuum up to ~340 K, leading to a pressure increase from $5 \cdot 10^{-9}$ to $1 \cdot 10^{-7}$ mbar, while the sample transformed into a white solid. Both observations suggested the evaporation of 1-iodo-1H,1H,2H,2H-perfluorohexane. At ~355 K the sample finally melted and ARXP spectra were recorded at 355 K as shown in Figure 3.4 for the C 1s, N 1s, F 1s, and I 3d regions in 0° (black) and 80° emission (gray). Calculated atom ratios from 0° emission data matched the nominal ratio within the margin of error, indicating a very low level of possible contamination. In the C 1s spectra, three signals are observed; the signals at 291.7 and 294.1 eV can be attributed to the CF_2 and CF_3 groups, respectively. All other carbons give rise to the signal at 286.7 eV (labelled C_{hetero}). By changing from 0° to

80° emission geometry, the F 1s signal as well as the CF_x signals increase in intensity, while the C_{hetero}, N 1s, and I 3d signal concurrently decrease, clearly indicating the preferential presence of the perfluorinated chains at the outer surface, while the imidazolium ring and the iodide lies below.

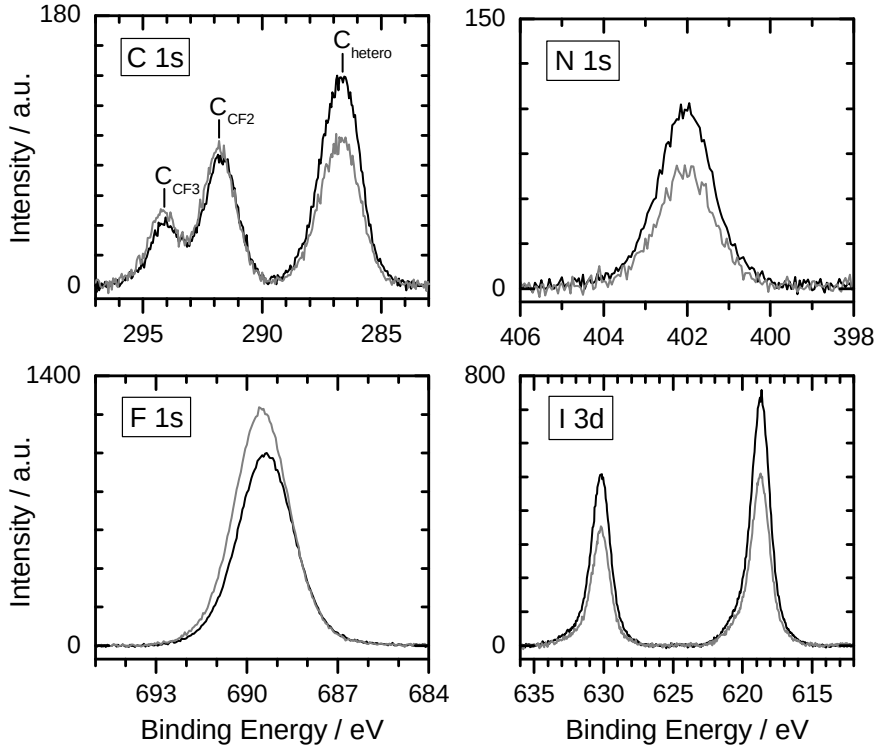

Figure 3.4. C 1s, N 1s, F 1s, and I 3d spectra of $[(CF_3(CF_2)_3(CH_2)_2)C_1Im]I$ in 0° (black) and 80° emission (gray) taken at ~355 K.

Chloroalkyl-functionalised ILs. **[P6]** Combined with either $[C_2C_1Im]^+$ or with $[C_8C_1Im]^+$ as counter ion, the 4-chlorobutylsulfonate anion $[ClC_4H_8SO_3]^-$ exhibits a very pronounced surface orientation. Hereto, the Cl 2p, O 1s and N 1s spectra of $[C_2C_1Im][ClC_4H_8SO_3]$ in 0° (black) and 80° emission (gray) are depicted in Figure 3.5. With increasing surface sensitivity (from 0° to 80°), an increase of the Cl 2p signal intensity is observed, while the O 1s signal of the sulfonate group decreases. The ARXPS characteristics of both end groups of the anion demonstrate the preferential orientation of the chlorobutyl chain oriented towards the vacuum, while the sulfonate group points bulkwards. The N 1s signal decreases simultaneous to the O 1s signal, suggesting a similar mean distance of the ionic head groups (SO_3^- group of the anion and imidazolium ring of the cation) to the outer surface.

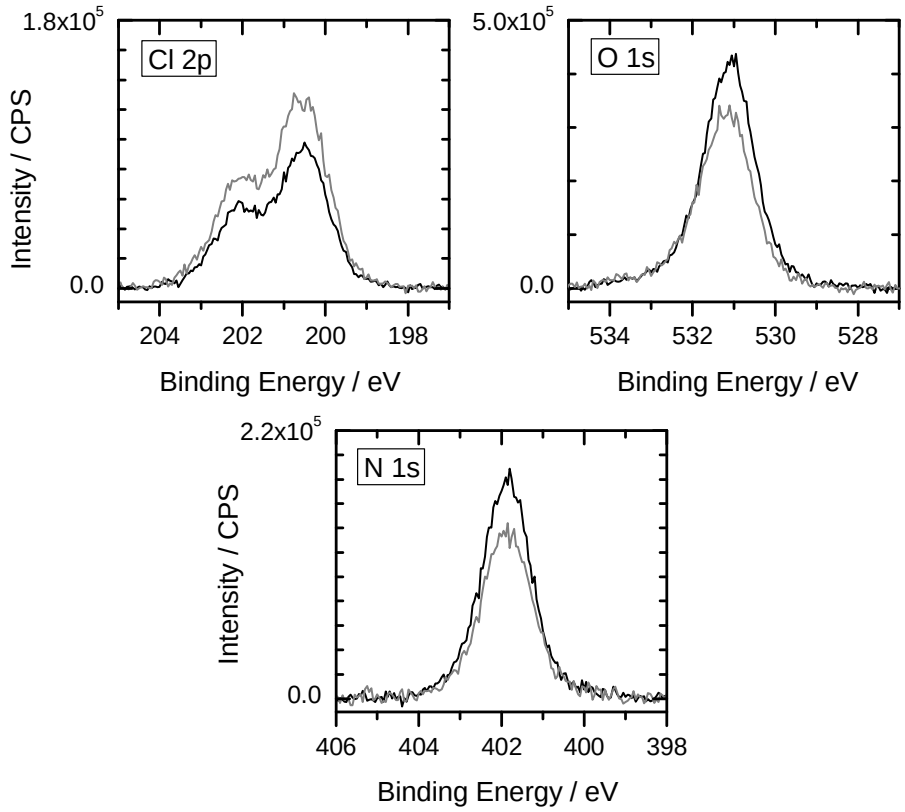

Figure 3.5. Cl 2p, O 1s, and N 1s spectra of $[C_2C_1Im][ClC_4H_8SO_3]$ in 0° (black) and 80° emission (gray).

***Amine-functionalised ILs.*[P6]** Figure 3.6 shows the N 1s spectra of the three amine-functionalised ILs $[(Me_2NC_3H_6)C_1Im][TfO]$, $[(Me_2NC_3H_6)C_1Im][Tf_2N]$, and $[(Me_2NC_3H_6)$-$PBu_3][FAP]$ in 0° (black) and 80° emission (gray). The N 1s signal of the amine-group (labelled N_{amine}) exhibits a binding energy of 399.3 eV. This signal is superimposed by the N 1s signal of the $[Tf_2N]^-$ anion (labelled N_{Tf2N}) in case of $[(Me_2NC_3H_6)C_1Im][Tf_2N]$. The second peak at higher binding energy (401.9 eV) belongs to the imidazolium nitrogens (labelled N_{imid}). Focusing first on the imidazolium-based systems, a slight increase in N_{amine} signal intensity and a slight decrease in the N_{imid} signal intensity are observed for 80° emission compared to 0°, revealing the excess presence of the amine groups at the outer surface, while the imidazolium rings and the anions lie below. With the phosphonium-based IL $[(Me_2NC_3H_6)PBu_3][FAP]$ no changes in N 1s intensity are observed when changing the emission angle, indicating an isotropic arrangement of the amine-functionalised cation at the surface.

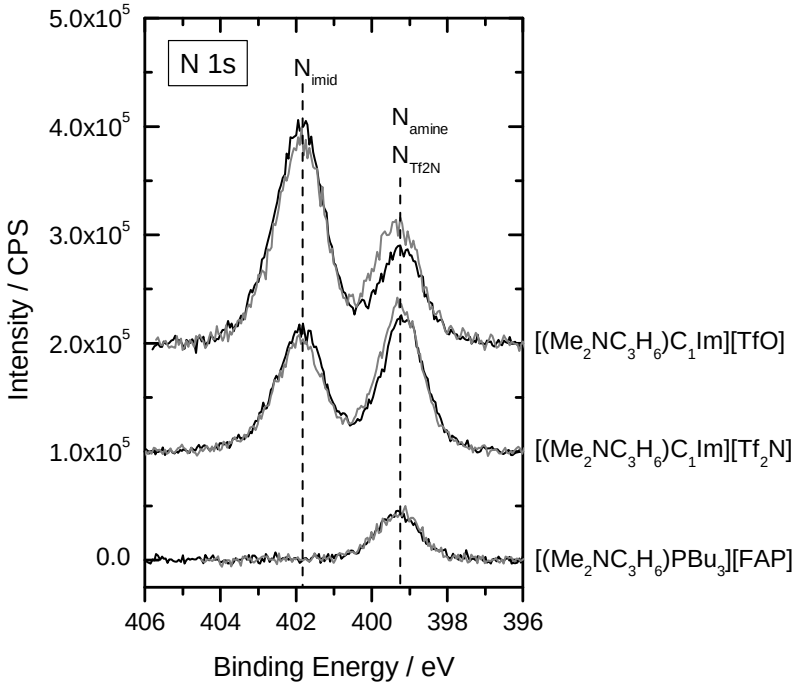

Figure 3.6. N 1s spectra of $[(Me_2NC_3H_6)C_1Im][TfO]$, $[(Me_2NC_3H_6)C_1Im][Tf_2N]$, and $[(Me_2NC_3H_6)$-$PBu_3][FAP]$ in 0° (black) and 80° emission (gray).

Ethylene glycol-functionalised ILs. In contrast to the above discussed functionalised ILs, the introduction of ethylene glycol groups into the side chain of an imidazolium leads to an isotropic arrangement of the functionalised ion at the surface. Hereto, in Figure 3.7 the C 1s and F 1s spectra of $[Me(EG)_2C_1Im][Tf_2N]$ are depicted in 0° (black) and 80° emission (gray). In the C 1s region, two signals are observed at 292.6 and 286.5 eV related to the CF_3-groups of the anion (labelled C_{Tf2N}) and from all carbons in the cation (labelled C_{hetero}), respectively. In contrast to the $[C_nC_1Im][Tf_2N]$ series, the differentiation between the carbon atoms of the imidazolium ring and the carbon atoms of the side chain is not possible as every carbon atom has at least one heteroatom (nitrogen or oxygen) as bonding partner. When going from 0° to 80° emission, no changes in intensity of the C_{hetero} peak is observed, strongly pointing towards an isotropic arrangement of the cation at the surface. Also, the surface tension of $[Me(EG)_2C_1Im][Tf_2N]$ (36.6 ± 0.7 mN m^{-1}) is much higher than for $[C_6C_1Im][Tf_2N]$ (30.2 ± 0.6 mN m^{-1}), confirming the isotropic arrangement, which is probably caused by the formation of intra- and intermolecular H-bonds between the oxygen atoms and the acidic hydrogens of the imidazolium ring.[26, 27]

Furthermore, the slight increase in F 1s intensity at 80° indicates a preferential surface orientation of the $[Tf_2N]^-$ anion in *cis*-conformation with its CF_3-groups pointing towards the vacuum. Consequently, the outer surface of $[Me(EG)_2C_1Im][Tf_2N]$ is not dominated by the

ether-functionalised hydrophilic alkyl chain but by the CF_3 groups contrary to the findings for $[C_nC_1Im][Tf_2N]$ for which the topmost surface layers are dominated by the alkyl chains. (Note that a similar arrangement of the ions at the surface was found for the ethylene glycol-functionalised ILs $[Me(EG)C_1Im][Tf_2N]$, $[Me(EG)_3C_1Im][Tf_2N]$, and $[Et(EG)_2C_1Im][Tf_2N]$.[P1, P3])

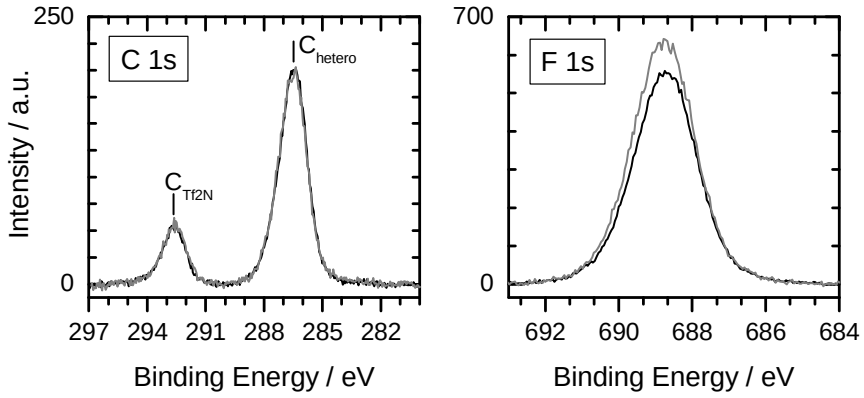

Figure 3.7. C 1s and F 1s spectra of $[Me(EG)_2C_1Im][Tf_2N]$ in 0° (black) and 80° emission (gray).

4. Surface segregation in ionic liquid mixtures and solutions

This chapter addresses the surface properties of different binary ionic liquid mixtures and the potential of tuning the solubility and surface enrichment of dissolved metal complexes by adding ligands to the system. The results of subchapters 4.1. and 4.4. have been published and only some highlights are summarised (the full papers [P2] and [P4] are presented in the Appendix). The other two subchapters 4.2 and 4.3 present additional unpublished results.

[P2] F. Maier, T. Cremer, **C. Kolbeck**, K. R. J. Lovelock, N. Paape, P. S. Schulz, P. Wasserscheid, H.-P. Steinrück
Insights into the Surface Composition and Enrichment Effects of Ionic Liquids and Ionic Liquid Mixtures
Phys. Chem. Chem. Phys. 12 (2010) 1905-1915.

[P4] **C. Kolbeck**, N. Paape, T. Cremer, P. S. Schulz, F. Maier, H.-P. Steinrück, P. Wasserscheid
Ligand Effects on the Surface Composition of Rh-Containing Ionic Liquid Solutions Used in Hydroformylation Catalysis
Chem. Eur. J. 16 (2010) 12083-12087.

The physical properties of ILs can be tuned for an individual application by changing the chemical nature of the cation, the anion or the substituents on the ionic head groups.[10] However, the desired physical properties are sometimes not achievable with neat ILs. For instance, the utilisation of a neat IL in electrochemical applications at sub-ambient temperature is limited as ILs possess high viscosities and, therefore, low ionic conductivities at low temperatures. Remedy for these shortcomings can be found in the usage of binary IL mixtures.[79-81] The mixing of two ILs will not only effect the bulk properties but also the surface properties. For an ideal mixture of two ILs a homogeneous distribution of the ions in the bulk and at the surface would be predicted. For real systems, however, it is expected that the component, which exhibits the lowest surface tension, will be enriched at the surface. Considering the dissolution of catalysts in ILs, such an enrichment of the catalyst at the surface would be advantageous for multiphase catalysis as the diffusion path ways of both reagent and product between catalyst and the liquid/gas interface would be minimised.

In the following, the ARXPS results of four different binary IL/IL mixtures will be presented. The influence of long alkyl chains attached to the imidazolium ring on the surface composition will be discussed in Chapter 4.1. The surface activity of different cationic head groups and anions will be probed in Chapters 4.2 and 4.3, respectively. Furthermore, in

Chapter 4.4, it will be shown that the surface activity of a transition metal complex can be influenced by its ligands.

4.1. Surface composition of a 9 : 1 binary mixture of $[C_2C_1Im][Tf_2N]$: $[C_{12}C_1Im][Tf_2N]$[P2]

In Chapter 3.1 it was shown that $[C_{12}C_1Im][Tf_2N]$ exhibits a lower surface tension than $[C_2C_1Im][Tf_2N]$ (29.8 ± 0.6 *vs.* 35.1 ± 0.7 mN m^{-1}). Therefore, one would expect that in a binary mixture of both ILs the $[C_{12}C_1Im]^+$ cation would be enriched at the surface, forming an $[C_{12}C_1Im][Tf_2N]$ layer. Furthermore, it is known from literature that long chain imidazolium cations segregate to the surface in aqueous solutions.[82, 83] If this segregation also takes place in a binary IL/IL mixture, is tested by the ARXPS measurement of a 9 : 1 mixture of $[C_2C_1Im][Tf_2N]$: $[C_{12}C_1Im][Tf_2N]$. The C 1s spectra of the 9 : 1 mixture, of neat $[C_2C_1Im][Tf_2N]$ and of neat $[C_{12}C_1Im][Tf_2N]$ are depicted in Figure 4.1a and b in 0° and 80° emission, respectively. As the nominal C_{alkyl} / C_{hetero} ratio of the 9 : 1 mixture is 2/5, which equals the ratio of neat $[C_3C_1Im][Tf_2N]$, the C 1s spectra of neat $[C_4C_1Im][Tf_2N]$ are added in Figure 4.1 ($[C_3C_1Im][Tf_2N]$ was not measured). In the 0° spectra, the 9 : 1 mixture exhibits a C_{alkyl} intensity that is higher than for $[C_2C_1Im][Tf_2N]$ but lower than for $[C_4C_1Im][Tf_2N]$; in other words, it has an intensity very close to that expected for $[C_3C_1Im][Tf_2N]$. Therefore, it can be concluded that the IL is an approximately homogeneous mixture with the expected stoichiometry within the probed near-surface region (7–9 nm).

At 80° emission, a clear enhancement of C_{alkyl} is observed for the mixture and the pure ILs. However, the C_{alkyl} signal intensity of the mixture is not larger than that of neat $[C_4C_1Im][Tf_2N]$, indicating an absence of the expected surface segregation of $[C_{12}C_1Im]^+$. This observation is confirmed by surface tension measurements of the 9 : 1 mixture: with a value of 33.4 ± 0.7 mN m^{-1} at 298.15 K the mixture exhibits a surface tension that is considerably closer to $[C_2C_1Im][Tf_2N]$ than to the value of pure $[C_{12}C_1Im][Tf_2N]$.

Contrary to our results, Souda *et al.* found a surface enrichment of $[C_8C_1Im]^+$ in the equimolar mixture of $[C_2C_1Im][PF_6]$ and $[C_8C_1Im][PF_6]$ with TOF-SIMS.[84] Also, surface tension measurements of binary IL/IL mixtures containing one cation with a long alkyl chain showed the segregation of this cation at the surface.[85-88] However, in all of these other studies small anions (like halides, $[NO_3]^-$, and $[BF_4]^-$) were used. Therefore, it is assumed that the molecular size of the anion plays a crucial role in the surface segregation of cations with long alkyl chains. With large anions like $[Tf_2N]^-$ the distance between the alkyl chains is

increased in comparison to the situation for small anions, which weakens the van-der-Waals interactions between the chains and, thereby, the tendency for aggregation at the surface.

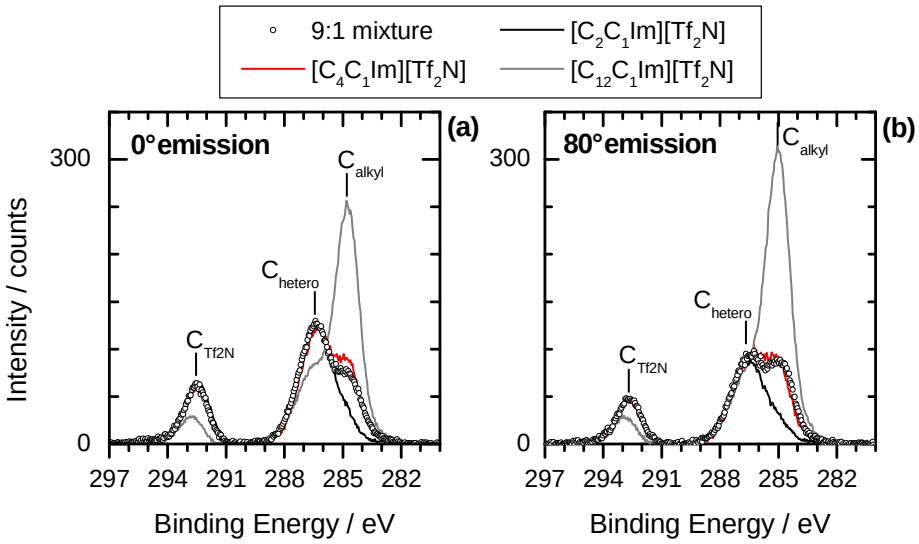

Figure 4.1. C 1s spectra in a) 0° and b) 80° emission of $[C_2C_1Im][Tf_2N]$, $[C_4C_1Im][Tf_2N]$, $[C_{12}C_1Im][Tf_2N]$, and the 9 : 1 binary mixture of $[C_2C_1Im][Tf_2N]$: $[C_{12}C_1Im][Tf_2N]$.

4.2. Influence of the cationic head group on the surface composition of binary IL/IL mixtures

To study the surface activity of different cationic head groups, two mixtures comprised of one anion and two cations are measured with ARXPS, namely a 0.26 : 0.74 mixture of trimethylsulfonium bis[(trifluoromethyl)sulfonyl]imide ($[S(CH_3)_3][Tf_2N]$) and $[C_2C_1Im][Tf_2N]$ and a 1 : 1 mixture of tributylmethylphosphonium methylsulfate ($[P_{4441}][MeOSO_3]$) and $[C_8C_1Im][MeOSO_3]$.

0.26 [S(CH₃)₃][Tf₂N] : 0.74 [C₂C₁Im][Tf₂N]. In Figure 4.2 the S 2p and N 1s spectra of the binary mixture 0.26 $[S(CH_3)_3][Tf_2N]$: 0.74 $[C_2C_1Im][Tf_2N]$ are depicted in 0° (black) and 80° emission (gray). In both regions two distinct signals can be observed. Considering the N 1s region, the signals at 401.2 and 398.7 eV can be attributed to the imidazolium nitrogens (N_{Im}) and to the $[Tf_2N]^-$ nitrogen (N_{Tf2N}), respectively. The S 2p signal at 168.1 eV ($2p_{3/2}$) stems from the two sulfur atoms in $[Tf_2N]^-$ (S_{Tf2N}), while the S 2p signal of the sulfonium cation exhibits a binding energy of 165.8 eV, which is in accordance with work of Zhang *et al.*, who measured XPS of cyclic sulfonium-based ILs.[89] The calculation of the chemical composition from the 0° emission spectra matches the nominal ratio of 0.26 : (2·0.74) within the margin of error. When going from 0° to 80° emission no distinct changes can be observed

in the N 1s and S 2p spectra, indicating the homogeneous distribution of the cations in the surface near-region and at the outer surface.

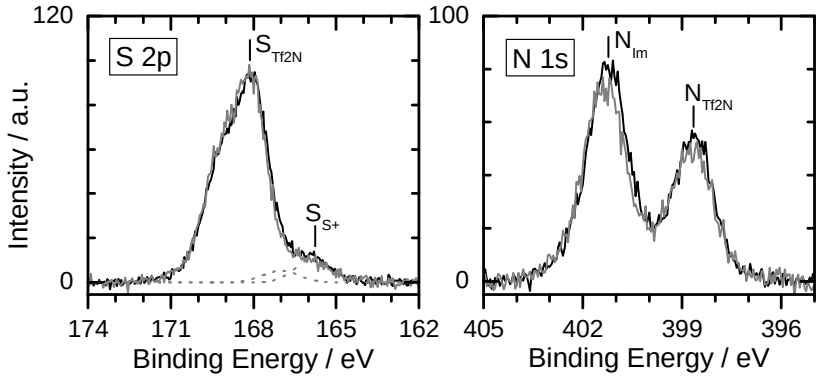

Figure 4.2. S 2p and N 1s spectra of the binary 0.26 : 0.74 mixture of $[S(CH_3)_3][Tf_2N]$ and $[C_2C_1Im][Tf_2N]$ in 0° (black) and 80° emission (gray). (The fit curves for the S_{S+} species in 0° emission are added as dotted lines for better clarity.)

1 : 1 [P$_{4441}$][MeOSO$_3$] : [C$_8$C$_1$Im][MeOSO$_3$]. In contrast to the above discussed mixture, the equimolar mixture of $[P_{4441}][MeOSO_3]$ and $[C_8C_1Im][MeOSO_3]$ shows changes in the core level spectra with emission angle. The corresponding P 2p, N 1s, C 1s, S 2p, and O 1s spectra of the mixture are depicted in 0° (black) and 80° emission (gray) in Figure 4.3. Two signals can be differentiated in the C 1s region at 284.8 and 286.4 eV. By comparison with the XP spectra of the neat ILs, the signal at 286.4 eV is attributed to carbon atoms which are bound to nitrogen or oxygen (labelled $C_{N,O}$); the signal at 284.8 eV stems from carbon atoms which either are bound to phosphor or have only carbon and hydrogen as bonding partner (labelled $C_{P,alkyl}$). In the O 1s region also two signals are observed; the terminal oxygen atoms of the sulfate group (O_{SO3}) exhibit an O 1s binding energy of 531.4 eV, while the O 1s signal of the bridging oxygen atom (O_{COS}) can be found at 533.0 eV. A summary of all components with their respective binding energies is given in Table 4.1. Additionally, Table 4.1 contains the nominal atom ratio as well as the calculated atom ratio (derived from the 0° spectra). As can be seen, the calculated atom ratio matches the nominal atom ratio within the margin of error, confirming the nominal concentration of the equimolar mixture.

Table 4.1. Binding energies E_B, nominal atom ratio and calculated atom ratio (derived from the 0° spectra) of the equimolar mixture of $[P_{4441}][MeOSO_3]$ and $[C_8C_1Im][MeOSO_3]$.

	P 2p	N 1s	C 1s ($C_{N,O}$)	C 1s ($C_{P,alkyl}$)	S 2p	O 1s (O_{COS})	O 1s (O_{SO3})
E_B [eV]	132.2[a]	401.6	286.4	284.8	168.0[a]	533.0	531.4
nominal atom ratio	0.5	1.0	3.5	10.0	1.0	1.0	3.0
0° emission atom ratio	0.5	1.0	3.7	10.4	1.1	1.0	3.2

[a]Binding energy of $2p_{3/2}$ component.

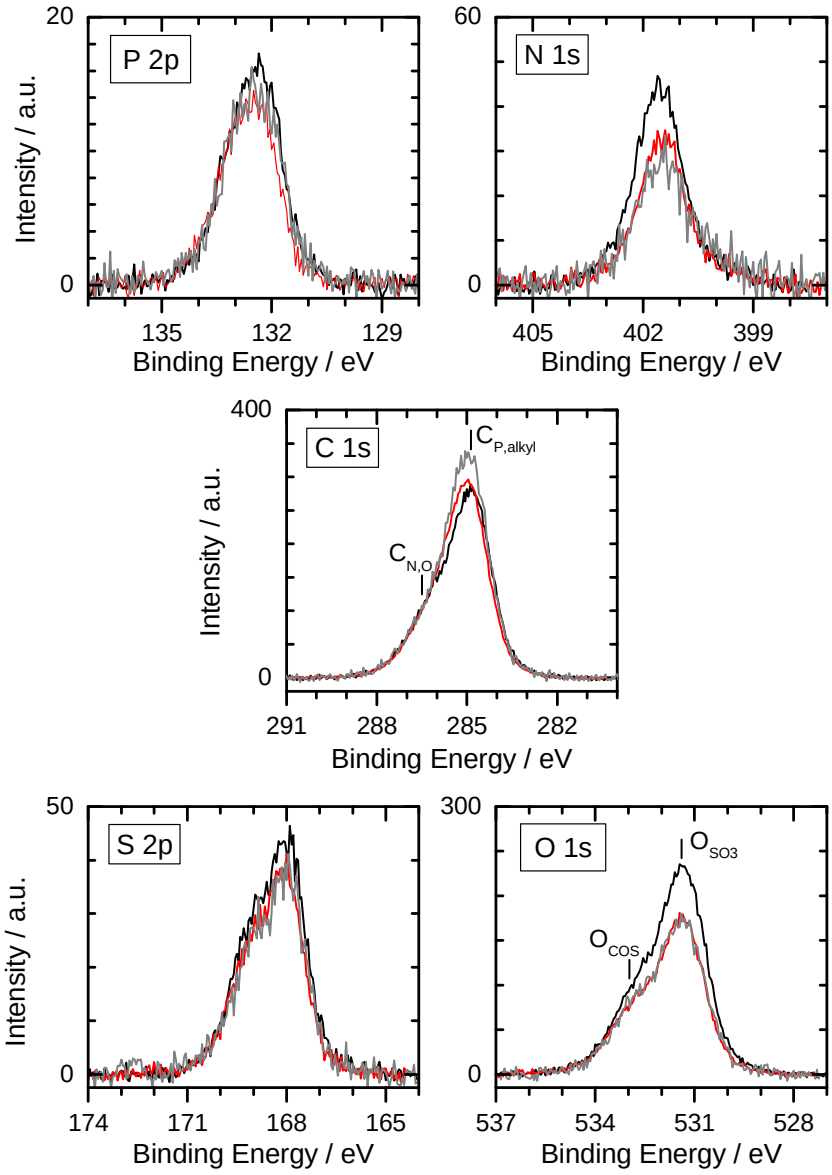

Figure 4.3. P 2p, N 1s, C 1s, S 2p, and O 1s spectra of an equimolar mixture of $[P_{4441}][MeOSO_3]$ and $[C_8C_1Im][MeOSO_3]$ in 0° (black) and 80° emission (gray). 80° spectra expected for an averaged surface composition (red) are calculated by summing the 80° signal intensities of both neat ILs and dividing it by two.

When going from 0° to 80° emission, an increase in $C_{P,alkyl}$ signal intensity is observed, while all other signals loose intensity. The stronger intensity decrease of the N 1s signal compared to P 2p initially suggests a surface enrichment of the phosphonium cation at expense of $[C_8C_1Im]^+$. However, the surface orientation of the ions at the surface has to be taken into account, which is probed by the ARXPS measurement of the neat ILs. While for $[P_{4441}]^+$ an isotropic arrangement is observed, $[C_8C_1Im]^+$ preferentially orientates itself at the surface with its octyl chain pointing towards the vacuum and the imidazolium head group towards the bulk (see Chapters 3.1 and 3.2). Furthermore, $[MeOSO_3]^-$ displays a preferential

orientation at the surface in both neat ILs: The methyl group sticks out towards the vacuum and the sulfate group points towards the bulk. To differentiate between orientation and enrichment effects in the mixture, averaged 80° spectra are calculated by taking the sum of the 80° signal intensities of both neat ILs and dividing it by two; the resulting curves are also displayed in Figure 4.3 (red line). Comparison of the red curves with the experimentally derived 80° spectra shows no differences in the S 2p and O 1s regions, indicating that the preferential surface orientation of $[MeOSO_3]^-$ is still present in the mixture. Interestingly, the 80° spectrum of the P 2p region matches the hypothetical red curve, but differences are seen in the C 1s and N 1s region: While for the experimentally derived $C_{P,alkyl}$ signal a higher intensity is observed, the N 1s signal shows less intensity compared to the hypothetical curve. Therefore, we assume that a slight surface enrichment of $[P_{4441}]^+$ at the expense of $[C_8C_1Im]^+$ takes place. The absence of an increased P 2p intensity compared to the hypothetical curve is attributed to a damping effect caused by the butyl substituents of the phosphonium cation.

4.3. Surface enrichment of anions containing perfluoroalkyl groups

As perfluorinated groups only exhibit weak intermolecular interactions, they show high surface activity in aqueous solutions.[28, 29] In the following, it will be shown that this surface activity is also seen in ionic liquid systems. Hereto, an equimolar mixture of $[C_2C_1Im][Pf_2N]$ and $[C_2C_1Im]I$ is probed with ARXPS. Due to the solid state of the mixture at room temperature, the sample was melted *in situ* at ~345 K to avoid charging effects in the XP spectra. In Figure 4.4, the respective F 1s, I 3d, O 1s, and N 1s regions are depicted in 0° (black) and 80° emission (gray). In the N 1s region two signals can be observed stemming from the imidazolium ring (N_{Im}) of the cation and the $[Pf_2N]^-$ anion (N_{Pf2N}) at 402.2 and 399.7 eV, respectively. To calculate the ratio of the ions $[C_2C_1Im]^+$, $[Pf_2N]^-$ and I^- in the surface, the $(0.5 \cdot N_{Im}) : N_{Pf2N} : I\ 3d$ ratio is considered: In 0° emission, a ratio of 2.0 : 1.3 : 0.7 is found instead of the nominal 2 : 1 : 1, indicating the enrichment of $[Pf_2N]^-$ in the first 7 - 9 nm of the IL surface at expense of iodide. This enrichment is more obvious in the 80° emission where an increase in F 1s intensity is observed, while the I 3d signal concurrently looses intensity, when going from 0° to 80° emission, resulting in a 1.9 : 1.7 : 0.4 ratio for $(0.5 \cdot N_{Im}) : N_{Pf2N} : I\ 3d$. These findings are particularly interesting for applications where the surface (but not the bulk) is needed to be decorated by the more expensive $[Pf_2N]^-$ anion: when mixing with the cheaper iodide anion, the more precious $[Pf_2N]^-$ is preferentially maintained at the outer surface. An analogous enrichment of perfluoroalkyl-containing anions

at the surface of ILs was also seen in a TOF-SIMS study of Souda *et al.*, who measured a 1 : 10 mixture of $[C_4C_1Im][Tf_2N]$: $[C_4C_1Im][PF_6]$.[84]

Despite the surface enrichment of $[Pf_2N]^-$, the N_{Pf2N} and O 1s intensities remain constant when going from 0 to 80° emission. This can be attributed to a density gradient from the surface to the bulk: The enrichment of the relative large $[Pf_2N]^-$ at the surface at expense of the small iodide results in a decrease in molar density in the surface layer. Therefore, the overall signal intensity in 80° emission is decreased as compared to 0° emission. This is directly reflected by the N_{Im} signal, which at 80° exhibits only ~75% of the 0° signal. Furthermore, the N_{Im} signal shows a slight shift towards higher binding energy when going form 0° to 80° emission (from 402.2 eV in 0° to 402.4 eV in 80° emission) which can also be explained by the enrichment of $[Pf_2N]^-$: An XPS study of different $[C_8C_1Im]^+$ based ILs showed the dependence of the imidazolium signals on the chemical nature of the anion, whereby the binding energy of the imidazolium signals shifted towards higher values with increasing anion size as the charge transfer from the anion to the cation decreased.[32, 90]

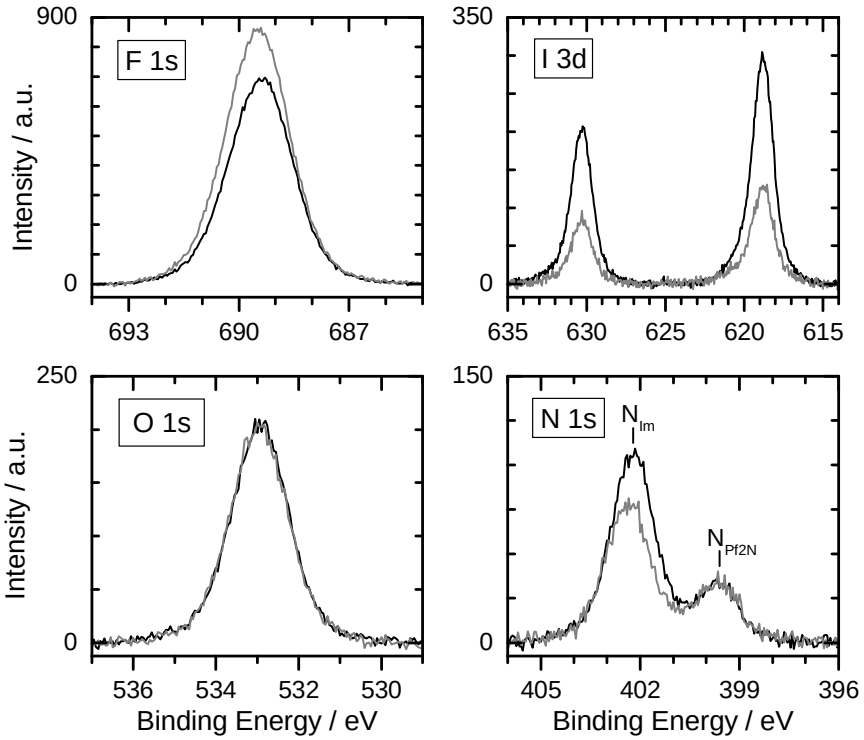

Figure 4.4. F 1s, I 3d, O 1s, and N 1s spectra of 1 : 1 mixture of $[C_2C_1Im][Pf_2N]$: $[C_2C_1Im]I$ in 0° (black) and 80° emission (gray).

As already mentioned above, the $(0.5 \cdot N_{Im})$: N_{Pf2N} : I 3d ratio in 80° emission amounts to 1.9 : 1.7 : 0.4, which suggests a slight excess of anions at the surface. This excess is also observed at the surface of neat $[C_2C_1Im][Pf_2N]$ and is attributed to a smaller mean distance of

$[Pf_2N]^-$ to the outer surface compared to $[C_2C_1Im]^+$. The $[Pf_2N]^-$ anion itself shows a preferential surface orientation as deduced from the F 1s and O 1s intensities: While the F 1s signal gains intensity when going from 0° to 80° emission, the O 1s intensity stays constant. These observations indicate a *cis*-conformation of the $[Pf_2N]^-$ anion at the surface with its perfluoroethyl groups pointing towards the vacuum, while the SO_2-groups point bulkwards. This preferential orientation is in accordance with the ARXPS results of neat $[(CF_3(CF_2)_3(CH_2)_2)C_1Im]I$ and $[Me(EG)_2C_1Im][Tf_2N]$ (see Chapter 3.3).

4.4. Influence of the ligand on the surface activity of transition metal complexes[P4]

This chapter addresses the modification of the surface activity of a transition metal complex by a ligand. Considering the saturated solution of (acetylacetonato)-dicarbonylrhodium(I) ($[Rh(acac)(CO)_2]$) in 3-ethyl-1-methylimidazolium ethylsulfate ($[C_2C_1Im][EtOSO_3]$), no Rh signal can be observed in the XP spectra as the Rh concentration (0.19 mol%) is below the detection limit of XPS. The absence of the Rh signal at 80° also rules out a surface enrichment of the Rh complex at the surface. Adding tris(3-sodium sulfonatophenyl)phosphine (Na_3tppts; 16.1 mol%) to $[C_2C_1Im][EtOSO_3]$ increases the maximum solubility of $[Rh(acac)(CO)_2]$ to 5.1 mol%, suggesting an *in situ* exchange of at least one CO ligand by tppts (see Scheme 4.1).

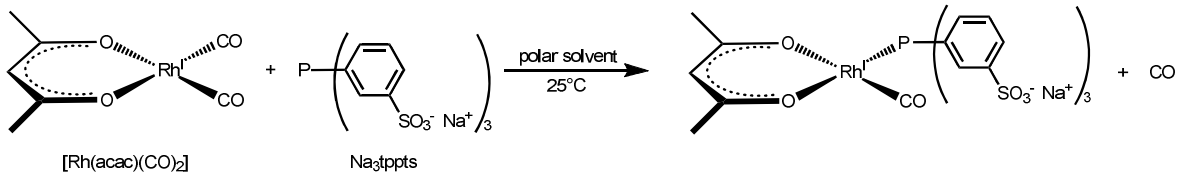

Scheme 4.1. Reaction of Na_3tppts with $[Rh(acac)(CO)_2]$ in polar solvents (according to ref. [91]).

The Rh 3d and C 1s spectra of the Rh-tppts solution are depicted in Figure 4.5 in 0° (black) and 80° emission (gray). The intensity ratio of the 0° emission spectra confirms the nominal Rh concentration of 5.1 mol%. However, when going from 0° to 80° emission an obvious intensity increase of the low binding energy signal (at ~285 eV) in the C 1s spectrum is observed. As this signal is mostly attributed to the benzene rings of the tppts ligands, the enrichment of tppts at the IL surface can be assumed. Due to this enrichment, all other XP signals are damped in 80° emission apart from the Rh 3d signal where an almost constant intensity is observed, indicating that next to „free“ tppts also the Rh-tppts complex is enriched

at the IL surface. These results confirm molecular dynamic simulations of Sieffert and Wipff, who claimed significant interface (surface) activity of Rh-tppts complexes in organic/ionic liquid (vacuum/IL) multiphase systems.[92, 93] By the calculation of the atomic ratios from the 80° spectra, a model of the surface of the Rh-tppts solution can be deduced (see Figure 4.5): The Rh-tppts complex as well as the „free“ tppts orientate themselves at the surface with their benzene rings pointing towards the vacuum, while the sulfonate groups and the phosphor point into the bulk. $[C_2C_1Im]^+$ acts as counterion of the sulfonate groups instead of Na^+, which is depleted into the bulk.

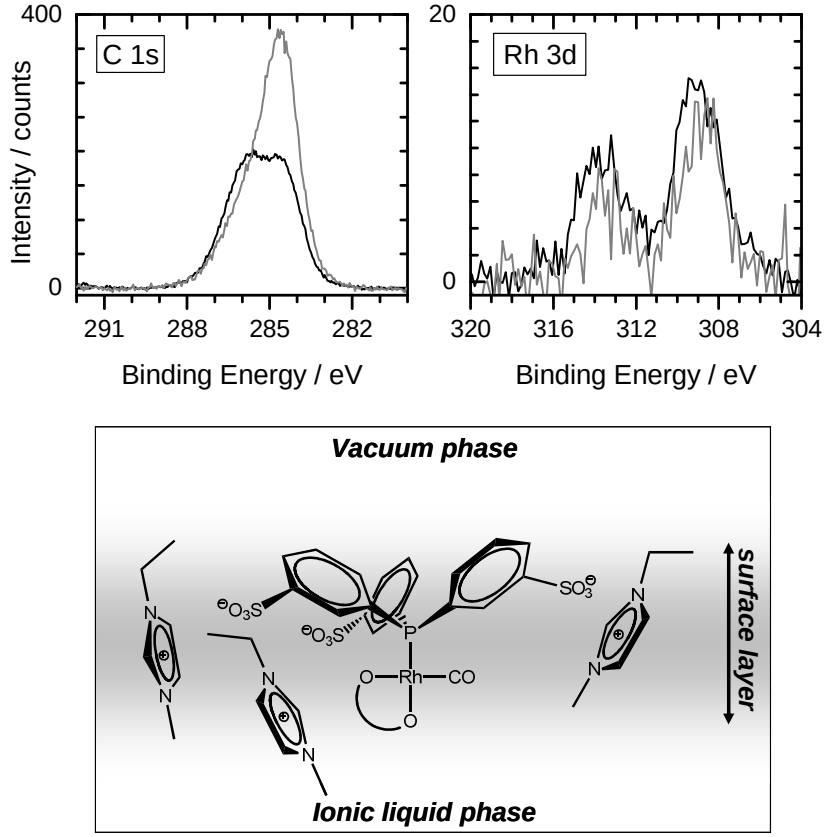

Figure 4.5. C 1s and Rh 3d spectra of a saturated solution of Na_3tppts in $[C_2C_1Im][EtOSO_3]$ with 5.1 mol% $[Rh(acac)(CO)_2]$ dissolved, taken at 0° (black) and 80° emission (gray). The graphical sketch at the bottom shows the proposed arrangement of the formed complex at the surface.

5. *in situ* XPS for monitoring of liquid-phase reactions

The application of *in situ* XPS as a tool for monitoring liquid-phase reactions is presented in this chapter. Examples of a nucleophilic substitution, an X-ray induced reduction, and a gas/IL interaction are discussed. Subchapters 5.1 and 5.2 summarise some highlights from already published data (see Appendix for full papers), while in Subchapter 5.3 unpublished results are presented.

[P5] **C. Kolbeck**, I. Niedermaier, N. Taccardi, P. S. Schulz, F. Maier, P. Wasserscheid, H.-P. Steinrück
Monitoring of Liquid-Phase Organic Reactions by Photoelectron Spectroscopy
Angew. Chem. Int. Ed. 51 (2012) 2610-2613.

[P6] I. Niedermaier, **C. Kolbeck**, N. Taccardi, P. S. Schulz, J. Li, T. Drewello, P. Wasserscheid, H.-P. Steinrück, F. Maier
Organic Reactions in Ionic Liquids Studied by in Situ XPS
ChemPhysChem 13 (2012) 1725-1735.

[P7] **C. Kolbeck**, N. Taccardi, N. Paape, P. S. Schulz, P. Wasserscheid, H.-P. Steinrück, F. Maier
Redox chemistry, solubility, and surface distribution of Pt(II) and Pt(IV) complexes dissolved in ionic liquids
accepted in J. Mol. Liq.

In addition to the steady-state analysis of the chemical composition of the near-surface region of ILs, XPS has the potential for monitoring reactions or other time-dependent processes (denoted "*in situ* XPS" in the following) within IL systems. This offers new possibilities to gain insight into reactions of liquid-phase systems. Information on surface composition and orientation, on different oxidation states in the proceeding reaction, and on the reaction kinetics under solvent-free ultraclean UHV conditions can be derived. Despite this great potential, the number of such studies is, however, very limited. The Licence group investigated the adsorption, dissolution and desorption of water on $[C_8C_1Im][BF_4]$ by temperature-programmed XPS.[94] They also studied the electrochemical generation of a Cu^+ species in a picolinium-based IL[95], and the electrochemical reduction of a haloferrate(III) IL dissolved in $[C_2C_1Im][EtOSO_3]$ to a haloferrate(II) compound.[96] The electrodeposition of potassium and rubidium metal from a pyrrolidinum-based IL was studied by Compton *et al.*[97, 98], whereas Kötz *et al.* addressed the influence of the applied potential on the binding energy and stability of $[C_2C_1Im][BF_4]$ with *in situ* electrochemical XPS.[99] Using IR and *in*

situ XP spectroscopy, Sobota *et al.* investigated the replacement of CO molecules pre-adsorbed at Pd nanoparticles on an Al_2O_3/NiAl(110) support by $[C_4C_1Im][Tf_2N]$.[100]

It typically requires at least one hour from the mixing of the reagents to the actual XPS measurement. Therefore, only reactions should be investigated, which can be triggered *in situ.* While for most of the above mentioned studies an electrochemical activation of the reaction was chosen, it is also possible to trigger the reaction thermally, photochemically or by dosage of a reactive gas, as will be shown in the following:

In Chapter 5.1 the results of the first *in situ* XPS monitoring of an organic, liquid-phase reaction are presented. In the course of this thermally-activated reaction a tertiary amine is alkylated by a chloroalkyl. Prior to the reaction, the reactive centres were linked to ionic head groups to drastically lower the vapour pressures of the reactants.

Platinum complexes are known to be photochemically active.[101] For neat Pt^{IV} salts a reduction to Pt^{II} is observed upon X-ray irradiation.[102, 103] In Chapter 5.2 results will be presented for IL solutions of Pt^{IV} and Pt^{II} salts, showing that the anion of the IL has a pronounced effect on the resulting oxidation state of platinum.

In Chapter 5.3 the interaction of NH_3 with the metal-containing IL 1-methyl-3-octylimidazolium trichlorocuprate(II) ($[C_8C_1Im][CuCl_3]$) is discussed. It will be shown that in addition to physisorption of NH_3 also chemisorption occurs.

5.1 Monitoring of a nucleophilic substitution[P5, P6]

The advantage of monitoring organic, liquid-phase reactions with *in situ* XPS, as compared to common analytical methods, such as NMR, is that all elements (apart from hydrogen and helium) can be quantified and analysed with respect to their chemical state (*e.g.*, oxidation state) within one experiment. To demonstrate the potential of *in situ* XPS, we have chosen a rather classic organic reaction, namely the nucleophilic substitution of a chloroalkyl by a tertiary amine. To drastically lower the vapour pressures of the reactants, the reacting groups are linked to ionic head groups. The corresponding functionalised ILs are depicted in Scheme 5.1a: the amine group is contained in the cation of **IL2** $[(Me_2NC_3H_6)C_1Im][TfO]$ and the covalently bound chlorine in the anion of **IL1** $[C_2C_1Im][ClC_4H_8SO_3]$ (note that the surface composition of both neat ILs was already discussed in Chapter 3.3). In the course of the reaction of **IL1** and **IL2**, the amine functionality of **IL2** is alkylated by the 4-chlorobutyl-sulfonate anion of **IL1** (Scheme 5.1b) to form the new zwitterionic salt **IL3**, and $[C_2C_1Im]$ [TfO] as the second product.

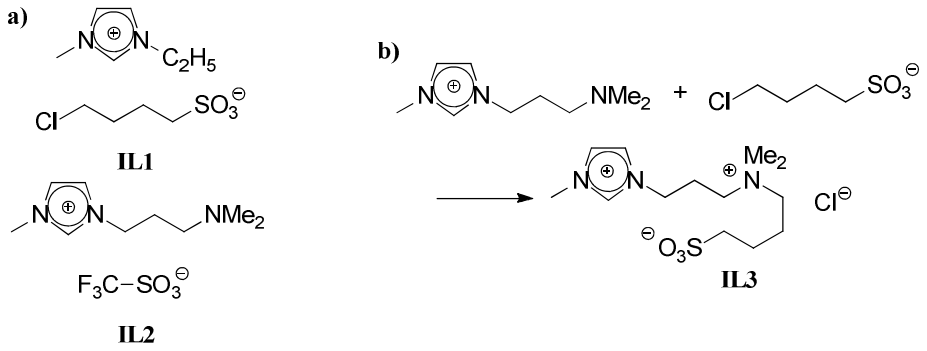

Scheme 5.1. a) Structure of **IL1** and **IL2**, and b) Alkylation of the amine group of **IL2** by the 4-chlorobutylsulfonate anion of **IL1** forming the alkylation product **IL3**.

As the reaction hardly proceeds at room temperature, the binary 1 : 1 mixture of the reactant ILs could be prepared under ambient conditions. This mixture was transferred into the XP spectrometer within 10 minutes and then heated. The Cl 2p and N 1s XP spectra in 0° emission before (black) and after (gray) heating the **IL1**/**IL2** mixture *in situ* at 100 °C for 2 hours and consecutive cooling to 60 °C are shown in Figure 5.1. In the 0° measurement before the reaction, the Cl $2p_{3/2}$ signal exhibits a binding energy of 200.2 eV which can be attributed to the covalently bound chlorine of **IL1** (labelled Cl_{cov}). In the N 1s region the two signals at 401.9 and 399.4 eV stem from the imidazolium nitrogens (N_{imid}) and the amine group (N_{amine}), respectively.

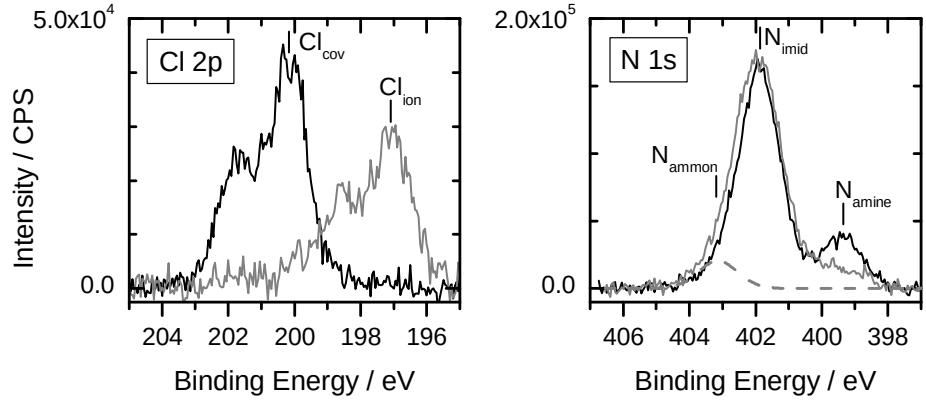

Figure 5.1. Cl 2p and N 1s spectra of 1 : 1 mixture of **IL1** and **IL2** in 0° emission before (black) and after (gray) heating to 100 °C for 2 hours and consecutive cooling to 60 °C.

After heating the mixture *in situ* to 100 °C distinct changes can be observed in the Cl 2p and N 1s regions in 0° emission. In the Cl 2p region, a loss in Cl_{cov} signal to ~9% of its former intensity is observed, indicating a (91 ± 5)% conversion of **IL1**. The signal of the formed chloride (Cl_{ion}) is found at a binding energy of 197.0 eV (for Cl $2p_{3/2}$). This binding energy matches the value found for $[C_8C_1Im]Cl$[104], confirming the ionic character of the formed

chlorine species. The overall loss in Cl 2p intensity of ~20% results from the surface enrichment of the more surface-active $[TfO]^-$ and the consequent depletion of chloride. A similar enrichment/depletion effect was already discussed in Chapter 4.3 within the study of the 1:1 mixture of $[C_2C_1Im]I$ and $[C_2C_1Im][Pf_2N]$.

The conversion of **IL2** can be monitored in the N 1s region: After heating, the N_{amine} intensity decreases to (44 ± 2)%, thus suggesting a (56 ± 3)% conversion of **IL2** to **IL3**. The loss in N_{amine} intensity is balanced by the broadening of the N_{imid} signal, which is attributed to the emerging ammonium group in **IL3**. By fitting the N 1s spectra to the three distinct nitrogen species, a binding energy of (403.1 ± 0.2) eV for this ammonium group N_{ammon} was found (see dashed line in Figure 5.1).

Comparison of the ~91% conversion of **IL1** and the ~56% of **IL2** indicates the existence of at least one concurrent reaction. Information on this reaction is obtained by studying the thermal stability of the neat ILs with *in situ* XPS. For **IL2** no changes are observed in the XP spectra after heating to 100 °C for 2 hours, verifying the thermal stability of the IL under the reaction conditions. The XP spectra of **IL1** after heating to 70 °C for 2 hours and to 100 °C for 1.5 hours, however, show distinct changes as evident from the comparison of the Cl 2p and O 1s spectra before (black) and after heating (gray) in Figure 5.2. Analogous to the mixture, a transformation of covalently bound chlorine to chloride is observed by the intensity loss in Cl_{cov} signal and the arising Cl_{ion} signal at 197.2 eV ($Cl\ 2p_{3/2}$). Furthermore, a concomitant decrease of the intensities of O 1s (Figure 5.2) and S 2p (not shown) is observed. These observations indicate that a reversal of the ring-opening reaction, which was employed to prepare **IL1**, occurs upon heating the IL in vacuum (see Scheme 5.2a). *In situ* mass spectrometry during the heating step shows the characteristic pattern of 1,4-butane sultone (in the gas phase), thus confirming the reverse reaction. Under standard pressure, however, this process does not occur until a temperature of ~215 °C[105], indicating the influence of the ultra-high vacuum conditions on the reaction equilibrium due to pumping away the evaporated 1,4-butane sultone.

For **IL1** the loss in Cl_{cov} intensity to ~45% after heating does not match the loss in O 1s intensity to ~58% of its former intensity. Therefore, a second reaction has to be taken into account. A possible explanation is the formation of a sulfonic acid ester by self-reaction of the 4-chlorobutylsulfonate (Scheme 5.2b). Because of the anionic nature the formed ester does not evaporate and, therefore, contributes to the O 1s signal.

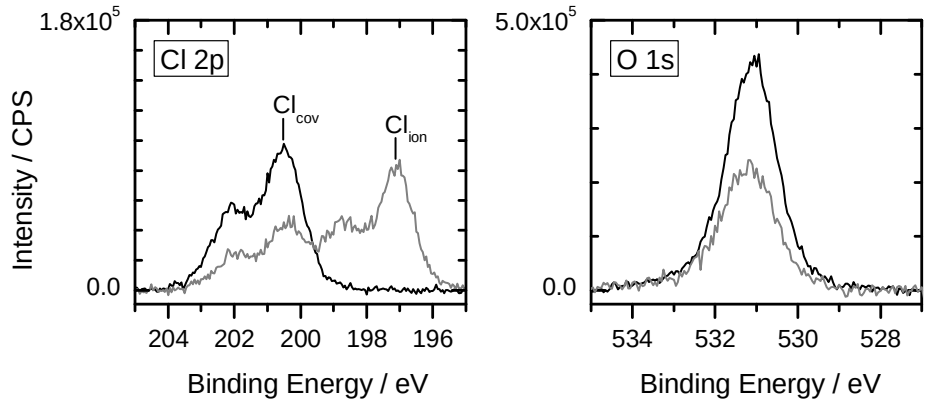

Figure 5.2. Cl 2p and O 1s spectra of neat **IL1** in 0° emission before (black) and after (gray) heating to 70 °C for 2 hours and to 100 °C for 1.5 hours.

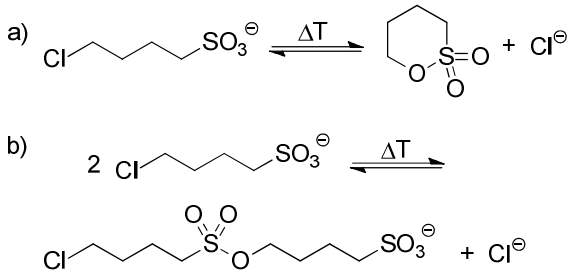

Scheme 5.2. a) Ring closing reaction of 4-chlorobutylsulfonate, forming 1,4-butane sultone and b) Formation of sulfonic acid ester by self-reaction of 4-chlorobutylsulfonate.

With the knowledge of the three possible reactions in the 1 : 1 mixture of **IL1** and **IL2** and by considering the intensity changes in the Cl 2p and N 1s spectra after heating the 1 : 1 mixture to 100 °C for 2 hours, the following percentage yield for the different products can be calculated for 4-chlorobutylsulfonate: ~56% alkylation product **IL3**, ~26% 1,4-butane sultone, and ~18% sulfonic acid ester. To verify the presence of the alkylation product **IL3** independently from the XPS results, electrospray-ionisation mass spectroscopy (ESI-MS) of the mixture after the above-described XPS measurement was conducted, resulting in a signal at m/z = 304.2, which can be unambiguously attributed to the **IL3** cation. The ESI-MS data was measured by Jing Li in the group of Prof. Thomas Drewello at the Chair of Physical Chemistry I at the University of Erlangen-Nuremberg.

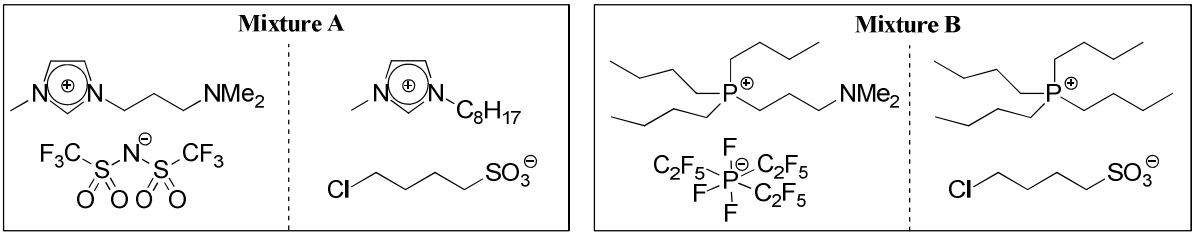

Scheme 5.3. Alternative mixtures tested for alkylation process.

The same alkylation reaction was tested also with the two mixtures depicted in Scheme 5.3. **Mixture A** is comprised of the same reactive ions but different counter ions ($[C_8C_1Im]^+$ instead of $[C_2C_1Im]^+$ as counter ion for $[ClC_4H_8SO_3]^-$; $[Tf_2N]^-$ instead of $[TfO]^-$ as counter ion of $[(Me_2NC_3H_6)C_1Im]^+$). The XPS analysis of **Mixture A** was not as straight forward as for the above-discussed mixture as the N_{amine} signal is superimposed by the N 1s signal of the $[Tf_2N]^-$ anion. Furthermore, upon heating the 1 : 1 mixture to 100 °C for 6 hours a precipitate is formed, which is attributed to the alkylation product. Due to this precipitation, most of the alkylation product leaves the surface-near region and, therefore, does not contribute to the XP spectra.

In **Mixture B** in Scheme 5.3, the $[TfO]^-$ anion of **IL2** was exchanged by $[FAP]^-$ and the imidazolium groups were exchanged by phosphonium groups, in order to remove the superimposition of the N_{imid} and N_{ammon} signals. However, no changes in the N 1s region are observed upon heating the 1 : 1 mixture to 100 °C for 1.5 hours. At the same time the covalently bound chlorine is completely transformed to chloride. This indicates that, while the alkylation reaction does not occur, all 4-chlorobutylsulfonate converts into 1,4-butane sultone and chloride. The inhibition of the alkylation reaction is possibly caused by steric hindrance of the amine-group by the neighbouring butyl chains of the phosphonium cation.

The presented results demonstrate the capability of XPS for monitoring of organic, liquid-phase reactions. For future studies, it appears feasible to also investigate the kinetics of organic liquid-phase reactions by following the evolution of a particular core level over time in isothermal experiments under XPS monitoring.[106] For such measurements, the data-collection time has to be reduced either by concentrating on one core level or by using high-intensity synchrotron radiation.[106] We anticipate that the herein described new method of investigating liquid-phase organic reactions can be transferred to many other organic transformations, apart from nucleophilic substitution reactions. As XPS represents an atom-specific, oxidation-state-specific, and surface-selective analysis technique, a significant amount of mechanistically relevant information on the surface region of reacting organic systems will become accessible with this approach.

5.2. X-ray induced redox-reactions of platinum-compounds dissolved in ionic liquids[P7]

X-rays and secondary electrons, which are produced upon X-ray irradiation, can lead to changes in the chemical nature of the studied substances in the course of an XPS experiment. Considering neat ILs, Keppler *et al.* showed in an XPS study of $[C_2C_1Im][Tf_2N]$ that cation and anion are destroyed by long-term X-ray irradiation.[107] For salts containing Cu^{II}, Co^{III}, Au^{III} or Pt^{IV}, the irradiation with X-rays leads to the reduction of the metal to a more stable oxidation state.[102] From these studies it is to be expected that the X-ray irradiation of IL solutions of Pt^{IV} compounds also leads to a reduction to a Pt^{II} species, analogous to neat Pt^{IV} salts.[102, 103] However, as will be shown in the following, the IL anion has a distinct influence on this reduction process.

One important issue was the solubility of the Pt complexes. While Pt-contents even below 0.01 mol% might be still sufficient for running catalytic reactions, the detection limit of XPS requires more than 0.2 mol% of Pt within the near surface region to obtain satisfactory signal-to-noise ratios. Hence, one important goal of this study was to increase the solubility of the metal complexes. For this purpose, Pt^{II} and Pt^{IV} salts with counter ions identical to the IL ions were employed in this study, namely $[Pt^{II}(NH_3)_4][Tf_2N]_2$ and $[C_2C_1Im]_2[Pt^{IV}Cl_6]$. In the course of our experiments, long term XPS studies of the solutions 3.57 mol% $[C_2C_1Im]_2[Pt^{IV}Cl_6]$ in $[C_2C_1Im][Tf_2N]$, 4.86 mol% $[C_2C_1Im]_2[Pt^{IV}Cl_6]$ in $[C_2C_1Im][EtOSO_3]$, and 4.45 mol% $[Pt^{II}(NH_3)_4][Tf_2N]_2$ in $[C_2C_1Im][Tf_2N]$ were conducted.

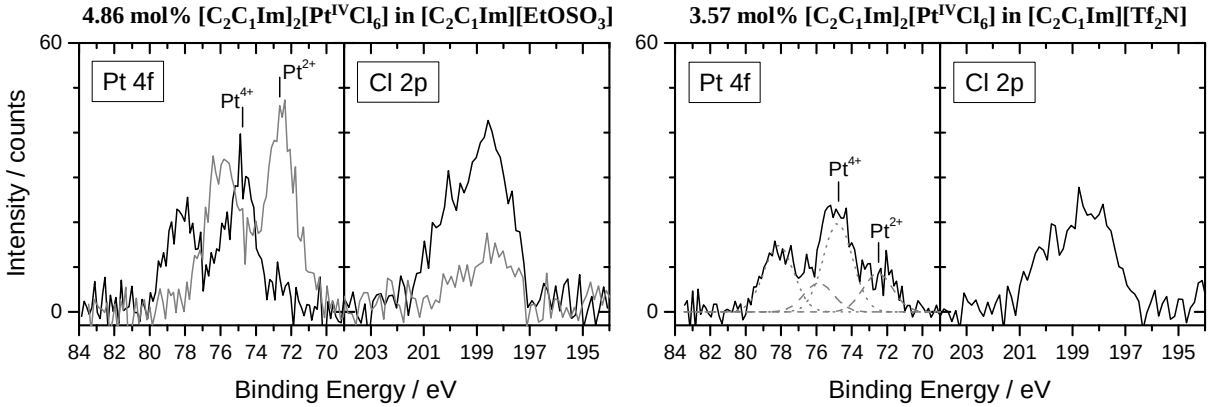

Figure 5.3. Pt 4f and Cl 2p spectra of 4.86 mol% $[C_2C_1Im]_2[Pt^{IV}Cl_6]$ in $[C_2C_1Im][EtOSO_3]$ (left side) and 3.57 mol% $[C_2C_1Im]_2[Pt^{IV}Cl_6]$ in $[C_2C_1Im][Tf_2N]$ (right side) in 0° emission taken right after introducing the sample in the X-ray beam (black) and after 414 min of X-ray irradiation (gray).

In the left side of Figure 5.3 the Pt 4f and Cl 2p spectra of $[C_2C_1Im]_2[Pt^{IV}Cl_6]$ dissolved in $[C_2C_1Im][EtOSO_3]$ are depicted; the spectra were taken at an emission angle of 0° right after introducing the sample into the X-ray beam (black) and after 414 min of X-ray irradiation

(gray). Considering the Pt 4f spectrum of the fresh sample, a binding energy of 74.8 eV is found for the main Pt $4f_{7/2}$ peak, which can be attributed to a Pt^{IV} species by comparison with literature data.[108] Next to the main Pt 4f doublet, a second, small doublet can be found at 72.6 eV ($4f_{7/2}$) stemming from a Pt^{II} species.[109] Upon prolonged X-ray irradiation, an intensity loss of the Pt^{IV} signal and a concomitant intensity increase of the Pt^{II} signal is observed; after 414 min the Pt^{IV} signal has nearly vanished and the Pt-concentration in the near-surface region has risen from 1.9 mol% at the beginning to 3.1 mol%, as calculated by the XP signal intensity ratios.

In the Cl 2p region also changes can be observed upon X-ray irradiation. As Pt^{II} prefers a square-planar coordination (with four chlorine ligands), a loss of the original Cl 2p signal (~198.5 eV for $2p_{3/2}$) of the octahedral coordinated complex (with six chlorine ligands) and the concurrent growth of an ionic Cl 2p signal at lower binding energies (~197.0 eV) is expected. The differentiation between the Cl 2p signals of the Pt^{II} and Pt^{IV} complex is not possible as they exhibit nearly the same binding energy. In the initial XPS measurement a Pt^{IV} : Pt^{II} : Cl ratio of $0.9 : 0.1 : (5.5 \pm 0.6)$ is observed, which matches the nominal 1.0 : 0 : 6.0 within the margin of error. However, after 414 min of X-ray irradiation a ratio of $0.1 : 0.9 : (1.2 \pm 0.1)$ is found, clearly demonstrating a loss of chlorine ligands; note that no free chloride could be detected in the Cl 2p region. Therefore, one can conclude that, in addition to the reduction of Pt^{IV} to Pt^{II}, also X-ray induced exchange of the chlorine ligand, most likely by the IL anion, occurs. The resulting free chloride either depletes into the bulk or evaporates as a volatile chlorine species like HCl (or Cl_2).

In contrast to the $[C_2C_1Im][EtOSO_3]$ solution, prolonged X-ray irradiation has no obvious effect on the XP spectra of 3.57 mol% $[C_2C_1Im]_2[Pt^{IV}Cl_6]$ in $[C_2C_1Im][Tf_2N]$. However, a Pt^{II} signal is observed next to the Pt^{IV} signal and a Pt^{IV} : Pt^{II} : Cl ratio of $0.7 : 0.3 : (4.1 \pm 0.4)$ is found already after only 15 min of X-ray irradiation (see right hand side of Figure 5.3), indicating the formation of a Pt^{II} species upon dissolution of the complex or less likely upon exposure to high vacuum. As the Pt^{II} signal intensity remains constant despite prolonged X-ray irradiation, it is concluded that X-ray induced processes do not play a role for the $[Tf_2N]^-$-based system. The decisive role of the IL anion for the efficiency of the X-ray induced reduction may be related to the different fragmentation pathways of $[EtOSO_3]^-$ and $[Tf_2N]^-$ upon electron irradiation. While radicals, formed by the reaction of electrons with $[Tf_2N]^-$, mainly decay by back recombination, the main product of the reaction between electrons and $[EtOSO_3]^-$ is the radical $CH_3{}^{\bullet}CHOH$, which is able to reduce the $[Pt^{IV}Cl_6]^{2-}$ complex.[110]

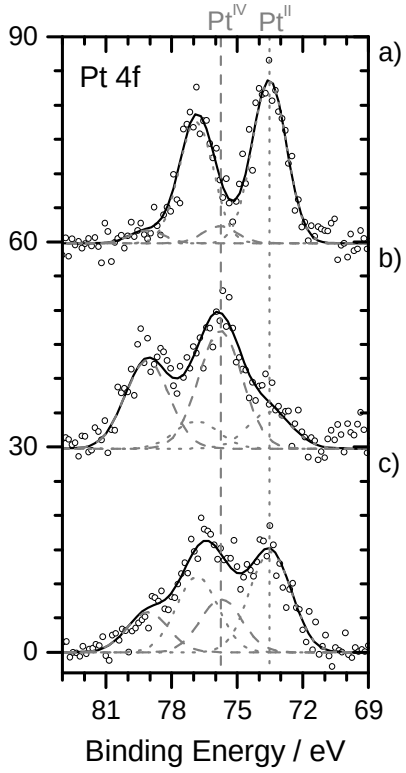

Figure 5.4. Pt 4f spectra of 4.45 mol% $[Pt^{II}(NH_3)_4][Tf_2N]_2$ in $[C_2C_1Im][Tf_2N]$ in 0° emission; spectra were taken right after introducing the sample in the X-ray beam (a), after 314 min of X-ray irradiation (b), and after removing the sample from the X-ray beam for ~18 hours (c).

In contrast to the above observed reduction process, an X-ray induced oxidation is observed for the solution of $[Pt^{II}(NH_3)_4][Tf_2N]_2$ in $[C_2C_1Im][Tf_2N]$; the respective Pt 4f spectra in 0° emission are depicted in Figure 5.4a,b. The Pt $4f_{7/2}$ signal (a) right after introducing the sample into the X-ray beam exhibits a binding energy of 73.5 eV, matching the value reported for $[Pt^{II}(NH_3)_4]Cl_2$ by Nefedov *et al.*[111] The X-ray irradiation of the sample for 314 min leads to an intensity increase of the Pt^{IV} signal at 75.4 eV, while the Pt^{II} signal concurrently decreases (b). After removing the sample from the X-ray beam for 18 hours the Pt 4f spectrum in Figure 5.4c was recorded. This spectrum clearly shows the partial recovery of the Pt^{II} species, possibly due to diffusion of still un-oxidised Pt^{II} to the surface and of Pt^{IV} into the bulk.

A possible explanation for the experimental observations may be the occurrence of a X-ray induced disproportionation of Pt^{II} into the observed Pt^{IV} species and a Pt^0 species [112,113], which most likely forms nanoparticles in the IL. These nanoparticles should have a high tendency to move from the IL surface into the bulk liquid, *i.e.*, out of the information depth of XPS, to be consistent with our data, as no signal for a Pt^0 species is observed in the Pt 4f spectrum.

5.3. Interaction of NH_3 with 1-methyl-3-octylimidazolium trichlorocuprate(II)

Significant attention is currently given to the utilisation of ILs as gas separation media; in this context, CO_2-capture from flue gases has the greatest prospect of success for industrial application.[30, 114, 115] Next to CO_2, NH_3 possesses a high solubility in ILs as well, as was shown for imidazolium-based[116, 117] and guanidinium-based ILs.[118] However, XPS measurements of these physisorbed systems are expected to be more or less impossible as the gas evaporates at the needed UHV conditions. Consequently, for our studies we chose the trichlorocuprate(II) IL $[C_8C_1Im][CuCl_3]$; for this system, chemisorption of NH_3 appeared possible. The used $[C_8C_1Im][CuCl_3]$ sample has a brown colour, is very viscous and has an inhomogeneous appearance with small solid flakes. These flakes are most probably comprised of $CuCl_2$ as $[C_8C_1Im][CuCl_3]$ is in equilibrium with its starting substances $[C_8C_1Im]Cl$ and $CuCl_2$ (see Scheme 5.4).

$$[C_8C_1Im][CuCl_3] \rightleftharpoons [C_8C_1Im]Cl + CuCl_2$$

Scheme 5.4. Equilibrium of $[C_8C_1Im][CuCl_3]$.

Before discussing the interaction of $[C_8C_1Im][CuCl_3]$ with NH_3, the surface composition of neat $[C_8C_1Im][CuCl_3]$ is addressed: the respective core level spectra (C 1s, N 1s, Cu $2p_{3/2}$, and Cl 2p) are depicted in Figure 5.5 in 0° (black) and 80° emission (gray). Due to the open shell configuration of Cu^{II}, the main Cu $2p_{3/2}$ peak at 934.2 eV is accompanied by a satellite, shifted ~9 eV towards higher binding energies. The peak assignment is done according to van der Laan *et al.*, who attributed the satellite to the final state $2p^53d^9$ and the main peak to the final state $2p^53d^{10}\underline{L}$, whereby $\underline{L}$ indicates that one electron is missing in the ligand valence state.[119] The structure of the satellite is caused by multiplet splitting into eight states due to J-J-coupling.[119] The Cu content is calculated by considering the N 1s : Cu $2p_{3/2}$ ratio, which amounts to 2.7 : 1.0 in 0° emission instead of the nominal 2 : 1. This clearly indicates that Cu is underrepresented in the detection range of XPS, *i.e.*, the first 7 - 9 nm of the surface of the inhomogeneous solution (see above).

In the C 1s region, the signal contains contributions of C_{hetero} and C_{alkyl} at 285.9 and 284.2 eV, respectively, analogous to Chapter 3.1. By going from 0° to 80° emission, the C_{alkyl} signal increases in intensity, indicating once again the orientation of the octyl chains towards the vacuum. All other XP signals are damped due to this enrichment of the octyl chains. However, the intensity decrease of Cu $2p_{3/2}$ to ~50% is stronger than for C_{hetero}, N 1s and

Cl 2p where only a decrease to ~76% is observed, suggesting the depletion of $[CuCl_3]^-$ from the surface at expense of chloride.

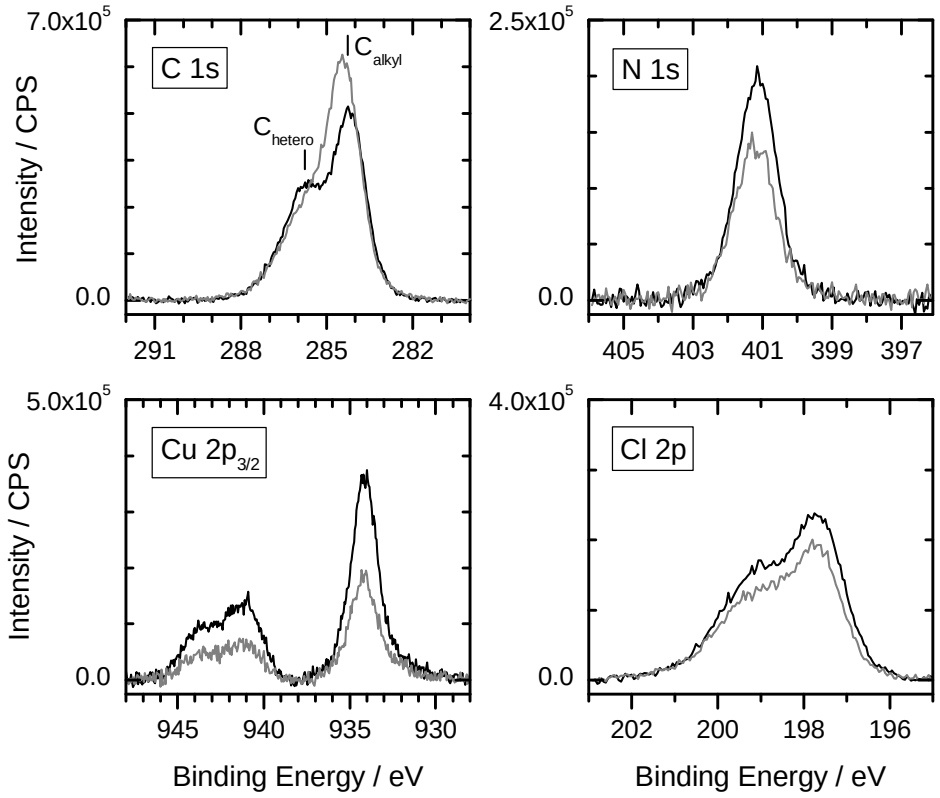

Figure 5.5. C 1s, N 1s, Cu $2p_{3/2}$, and Cl 2p spectra of $[C_8C_1Im][CuCl_3]$ in 0° (black) and 80° emission (gray).

To study the interaction of NH_3 with $[C_8C_1Im][CuCl_3]$, the sample was cooled to ~90 K and NH_3 was dosed ($1 \cdot 10^{-6}$ mbar, 5 min) onto the frozen sample resulting in multilayer adsorption of NH_3 with a thickness greater than 9 nm. By moderate heating to ~125 K the multilayer desorbed, leaving behind a thin layer of NH_3. This can be comprehended in the N 1s spectrum where one broad signal can be observed (see Figure 5.6). This signal can be deconvoluted into equal contributions of the imidazolium nitrogens (labelled N_{Im}) and NH_3 (labelled N_{NH3}) at 401.2 and 399.3 eV, respectively. The N_{NH3} signal looses intensity continuously by heating slowly to ~205 K, where a 4.4 : 1 ratio for N_{Im} : N_{NH3} is observed. In the course of heating to ~224 K the sample liquefied. Residual NH_3 is still visible in the XP spectra at ~224 K and desorbs almost completely at ~245 K.

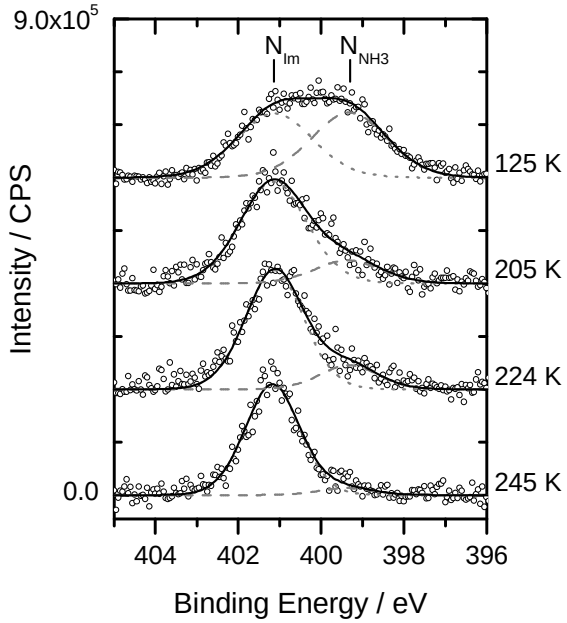

Figure 5.6. Thermal evolution of the N 1s spectra of $[C_8C_1Im][CuCl_3]$ after dosing NH_3 ($1 \cdot 10^{-6}$ mbar, 5 min) at 90 K. (Margin of error for temperature is ± 10 K.)

To distinguish between physi- and chemisorption, the Cu $2p_{3/2}$ signal is considered. The analysis is complicated by the fact that upon prolonged X-ray irradiation a second Cu $2p_{3/2}$ signal at 931.9 eV is observed, which stems either from a Cu^I or Cu^0 species, indicating the X-ray induced reduction of Cu^{II}; a differentiation between the Cu^I and Cu^0 is not possible as both exhibit very similar binding energies.[120] To avoid beam damage, a non-irradiated $[C_8C_1Im][CuCl_3]$ sample was prepared by cooling to ~229 K and dosing NH_3 (7 min, $1 \cdot 10^{-6}$ mbar) before the XPS measurement; the respective N 1s and Cu $2p_{3/2}$ spectra in 0° emission are depicted in Figure 5.7 (gray). Additionally, the N 1s and Cu $2p_{3/2}$ spectra of $[C_8C_1Im][CuCl_3]$ at room temperature are included in Figure 5.7 (black). To enable a direct comparison the spectra were normalised to the N_{Im} intensity. In the N 1s spectrum of the NH_3-pretreated sample the N_{NH3} peak at 399.3 eV is once again observed with an intensity ratio of 4.3 : 1 for N_{Im} : N_{NH3}. Upon adsorption of NH_3 the multiplet splitting of the Cu $2p_{3/2}$ satellite is affected: the higher binding energy components gain intensity relative to the lower binding energy components. This influence of NH_3 on the structure of the satellite suggests that NH_3 is interacting with Cu^{II} and that NH_3 is chemisorbed in $[C_8C_1Im][CuCl_3]$. Furthermore, the Cu $2p_{3/2}$ signal gains intensity in comparison to the untreated sample, indicating a higher content of Cu^{II} in the surface-near region upon NH_3 adsorption. A temperature effect can be excluded, as the XP spectra of the untreated $[C_8C_1Im][CuCl_3]$ exhibit the same Cu $2p_{3/2}$: N_{Im} ratio at ~230 and 300 K.

To calculate the adsorption enthalpies of the chemisorbed and physisorbed species it is desirable to conduct a more precise temperature programmed desorption (TPD) experiment in the future, to avoid the X-ray induced reduction of Cu^{II}.

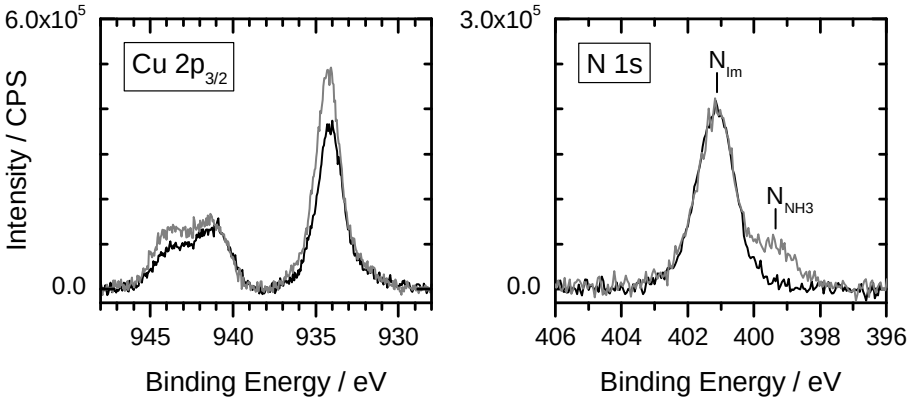

Figure 5.7. Cu $2p_{3/2}$ and N 1s spectra of $[C_8C_1Im][CuCl_3]$ before dosing NH_3 at 300 K (black) and after dosing NH_3 ($1 \cdot 10^{-6}$ mbar, 7 min) at 229 ± 10 K (gray).

6. Conclusions

The application of ILs as media in multiphase catalysis (*e.g.*, in the SILP process), has been the motivation to study the surface properties of IL systems. By employing ARXPS, the surface composition of these IL systems was obtained in a qualitative and quantitative way, which enabled statements about surface orientation and enrichment effects. Furthermore, it was shown that *in situ* XPS can be applied to monitor liquid-phase reactions and can also be adapted in the future to study SILP reactions.

Orientation of IL ions at the surface

Several imidazolium-based ILs were studied with ARXPS to obtain an understanding of the surface orientation of the ions with respect to their chemical structure. The ARXPS results of $[C_nC_1Im][Tf_2N]$ ILs (n = 1, 2, 4, 6, 8, 10, 12, 16) unambiguously demonstrate that, for a chain length of $n \geq 4$, the cation preferentially orientates itself within the surface layer with its alkyl chains pointing towards the vacuum, forming an aliphatic overlayer above an ionic sublayer, which consists of the cationic head groups and the anions. This double layer structure is also observed when introducing perfluoroalkyl chains, alkyl chains with terminal chlorine, or tertiary amine groups into the IL structure. However, the implementation of ether groups into the alkyl chain results in an isotropic arrangement at the surface, which can be ascribed to the formation of H-bonds between the ether groups and the acidic hydrogen atoms of the imidazolium ring.[26, 27]

Preferential surface orientation also affects the surface tension; according to the "Langmuir principle", only those chemical groups that form the outer surface contribute to the surface tension.[40] In case of the $[C_nC_1Im][Tf_2N]$ system, the cationic head group and the anion will contribute less and less to the surface tension with increasing alkyl chain length, due to the increasing thickness of the aliphatic overlayer at the surface. This results in the observed reduction of the surface tension from 36.3 ± 0.7 mN m^{-1} for $[C_1C_1Im][Tf_2N]$ to 29.5 ± 0.6 mN m^{-1} for $[C_8C_1Im][Tf_2N]$. For $[Me(EG)_2C_1Im][Tf_2N]$ a surface tension value of 36.6 ± 0.7 mN m^{-1} is found, which is much higher than for the non-functionalised IL of similar chain length $[C_6C_1Im][Tf_2N]$ (30.2 ± 0.6 mN m^{-1}), confirming the isotropic arrangement of $[Me(EG)_2C_1Im]^+$ at the surface.

In contrast to the $[C_nC_1Im][Tf_2N]$ system, variation of the anion in the system $[C_8C_1Im]X$ does not lead to a simple correlation between the surface tension and the surface orientation.

In fact, differences in the surface tension could mainly be ascribed to changes in the bulk intermolecular interaction energies.

Surface enrichment effects in ionic liquid systems

In mixtures and solutions, it is expected that the component, which contributes to a lowering of the surface tension, will be enriched at the surface. However, in the ARXPS measurement of a 9 : 1 binary mixture of $[C_2C_1Im][Tf_2N]$: $[C_{12}C_1Im][Tf_2N]$, a homogeneous distribution of the cations at the surface was found instead of a preferential surface segregation of the $[C_{12}C_1Im]^+$ cation. As other groups[84-88], who measured analogous systems with smaller anions, showed the occurrence of a surface segregation of the long alkyl chain component, it is assumed that the molecular size of the anion plays a crucial role in the surface segregation of cations with long alkyl chains.

For the equimolar mixture of $[C_2C_1Im]I$ and $[C_2C_1Im][Pf_2N]$, *i.e.*, a system of short-chained cations and very different anions, a clear surface enrichment of $[Pf_2N]^-$ at expense of iodide was observed, which can be explained by the high surface activity of the perfluoroalkyl groups. Other equimolar mixtures of ILs, consisting of the same anion and different cationic head groups, showed either only a slight surface enrichment of $[P_{4441}]^+$ in the $[P_{4441}][MeOSO_3]$/$[C_8C_1Im][MeOSO_3]$ mixture or an homogeneous distribution of the cations in the $[S(CH_3)_3][Tf_2N]$/$[C_2C_1Im][Tf_2N]$ mixture.

For solutions of catalytically active Rh complexes in $[C_2C_1Im][EtOSO_3]$, it was demonstrated that the surface activity of the complex is clearly dependent on its ligands. The precursor $[Rh(acac)(CO)_2]$ exhibits no surface activity in $[C_2C_1Im][EtOSO_3]$. By co-dissolving $[Rh(acac)(CO)_2]$ in a solution of Na_3tppts in $[C_2C_1Im][EtOSO_3]$, at least one CO ligand is exchanged by a tppts ligand, which itself is enriched at the surface of $[C_2C_1Im]$ $[EtOSO_3]$. With the introduction of the surface-active tppts ligand into the Rh complex, the surface activity of the Rh-tppts complex is increased, leading to an excess of Rh at the surface.

Monitoring of liquid-phase reactions with in situ XPS

The change of core level binding energies with the chemical state of the elements enables the monitoring of reactions with *in situ* XPS. By linking the reactive groups to an ionic head group, we were even able to follow an organic liquid-phase reaction between $[(Me_2NC_3H_6)$-$C_1Im][TfO]$ and $[C_2C_1Im][ClC_4H_8SO_3]$. In course of the reaction, covalently bound chlorine was substituted by the tertiary amine group, forming chloride and an ammonium group. These changes in charge induced distinct shifts in the Cl 2p and N 1s regions. We were able to

quantify that only ~56% of $[ClC_4H_8SO_3]^-$ participated in this substitution reaction under the applied UHV conditions. As parallel reactions, the formation of an anionic sulfonate ester and the intramolecular elimination of volatile sultone from the anion $[ClC_4H_8SO_3]^-$ could be identified by the quantitative XPS analysis.

Another type of reaction, that was investigated by *in situ* XPS, was related to the rather complex phenomenon of X-ray induced reduction and oxidation processes of platinum salts in ILs with the focus on the reduction of the Pt^{IV} salt $[Pt^{IV}Cl_6]^{2-}$ in $[EtOSO_3]^-$ and $[Tf_2N]^-$ ILs. While in $[C_2C_1Im][EtOSO_3]$ a complete reduction of $[Pt^{IV}Cl_6]^{2-}$ to Pt^{II} was witnessed by changes in Pt 4f and Cl 2p core levels, only about 30% of Pt^{IV} changed to Pt^{II} in $[C_2C_1Im][Tf_2N]$. One reason for the less pronounced radiation induced reduction behaviour of Pt^{IV} in $[Tf_2N]^-$ ILs is possibly related to the nature of the radicals formed by the reaction of secondary electrons with the IL anions. While the radicals of $[Tf_2N]^-$ mainly decay by back recombination, the reaction of electrons and $[EtOSO_3]^-$ mainly results in $CH_3{}^{\bullet}CHOH$ radicals, which are able to reduce the $[Pt^{IV}Cl_6]^{2-}$ complex.[110]

Finally, the interaction of gaseous NH_3 with the IL $[C_8C_1Im][Cu^{II}Cl_3]$ was probed with *in situ* XPS as an example for an IL-gas interface under vacuum conditions. Multilayer physisorption of NH_3 was carried out at a sample temperature of ~90 K with an NH_3 background pressure around 10^{-6} mbar. Annealing to ~125 K led to the multilayer desorption, with a remaining thin layer of NH_3 on top of the frozen IL sample. Residual NH_3 was still observed after heating to ~224 K, where the sample changed into its liquid state. A complete desorption of NH_3 occurred at a temperature of ~245 K. A closer look at the Cu $2p_{3/2}$ signal revealed changes in the satellite structure upon NH_3 adsorption, which indicated a chemisorbed NH_3 species.

Zusammenfassung

In der Mehrphasenkatalyse, z. B. in „Supported Ionic Liquid Phase“ (SILP) Prozessen mit ionischen Flüssigkeiten (ILs) als Lösungsmittel, spielen Grenzflächen, insbesondere die Grenzfläche IL/Gasphase, eine wesentliche Rolle. Diese Doktorarbeit beschäftigte sich deshalb mit grundlegenden Oberflächeneigenschaften von IL-Systemen. Die qualitative sowie quantitative Analyse der Oberflächenzusammensetzung unterschiedlichster IL-Systeme erfolgte hauptsächlich mittels winkelaufgelöster Photoelektronenspektroskopie (ARXPS) im Ultahochvakuum (UHV). Dadurch wurden Orientierungseffekte sowie präferentielle Segregationseffekte bestimmter Komponenten in den obersten Molekülschichten bestimmt. Weiterhin konnte anhand verschiedener Beispiele gezeigt werden, dass *in situ* XPS zur Verfolgung von Reaktionen in flüssiger Phase und zukünftig auch zur Untersuchung von SILP Reaktionen verwendet werden kann.

Orientierung der IL-Ionen an der Oberfläche

Der Zusammenhang zwischen Oberflächenorientierung und chemischer Struktur der Ionen in ILs wurde mit ARXPS an einigen Imidazolium-basierten ILs untersucht. Die Messungen am System $[C_nC_1Im][Tf_2N]$ (n = 1, 2, 4, 6, 8, 10, 12, 16) zeigten, dass ab einer Kettenlänge von $n = 4$ eine präferentielle Orientierung des Kations an der Oberfläche vorliegt. Während die Alkylketten in Richtung Vakuum zeigen und eine aliphatische Deckschicht ausbilden, liegen die kationischen Kopfgruppen und die Anionen darunter. Diese Schichtstruktur wurde auch für ILs mit perfluorierten oder chlorierten Alkylketten sowie bei Funktionalisierung der Kette mit einem tertiären Amin beobachtet. Dagegen führt der Einbau von Ethergruppen in die Alkylkette zu einer isotropen Anordnung des Kations an der Oberfläche, vermutlich aufgrund der Ausbildung von Wasserstoffbrücken zwischen den Ethergruppen und den acidischen H-Atomen am Imidazolium-Ring.[26, 27]

Orientierungseffekte an der IL Oberfläche wirken sich auch auf die Oberflächenspannung aus; gemäß dem Prinzip von Langmuir tragen nur die chemischen Gruppen, welche sich an der äußeren Oberfläche befinden, zur Oberflächenspannung bei.[40] Im Fall des $[C_nC_1Im][Tf_2N]$ Systems ist daher der Beitrag der kationischen Kopfgruppen und der Anionen zur Oberflächenspannung umso geringer, je länger die Alkylkette wird, da mit steigender Kettenlänge die Dicke der aliphatischen äußeren Schicht zunimmt. Dadurch reduziert sich die Oberflächenspannung von 36.3 ± 0.7 mN m^{-1} für $[C_1C_1Im][Tf_2N]$ auf 29.5 ± 0.6 mN m^{-1} für

$[C_8C_1Im][Tf_2N]$. Für $[Me(EG)_2C_1Im][Tf_2N]$ wurde eine Oberflächenspannung von 36.6 ± 0.7 mN m^{-1} gefunden; diese ist deutlich höher als die des ähnlich großen $[C_6C_1Im][Tf_2N]$ (30.2 ± 0.6 mN m^{-1}), was zusätzlich für die isotrope Anordnung des $[Me(EG)_2C_1Im]^+$ Kations an der Oberfläche spricht.

Im Gegensatz zum $[C_nC_1Im][Tf_2N]$ System wurde bei Variation des Anions im System $[C_8C_1Im]X$ keine einfache Korrelation der Oberflächenspannung mit der Oberflächenorientierung beobachtet. Aufgrund des sehr unterschiedlichen Aufbaus der Anionen dominieren in diesen Systemen die intermolekularen Wechselwirkungen im Volumen, womit die unterschiedlichen Oberflächenspannungswerte größtenteils erklärt werden konnten.

Oberflächenanreicherungen in IL-Systemen

In Mischungen und Lösungen erwartet man eine Anreicherung der Komponente mit der geringsten Oberflächenspannung an der Oberfläche. Entgegen dieser Erwartung zeigten ARXPS Messungen einer 9 : 1-Mischung der ILs $[C_2C_1Im][Tf_2N]$ und $[C_{12}C_1Im][Tf_2N]$ eine homogene Verteilung der Kationen an der Oberfläche anstatt einer Oberflächensegregation des $[C_{12}C_1Im]^+$ Kations. Andere Arbeitsgruppen[84-88], die analoge Systeme mit kleineren Anionen untersuchten, beobachteten dagegen eine Anreicherung der langkettigen Komponente an der Oberfläche. Dies deutet darauf hin, dass die chemische Struktur des Anions eine entscheidende Rolle bei der Oberflächensegregation spielt.

Für die äquimolare Mischung von $[C_2C_1Im]I$ und $[C_2C_1Im][Pf_2N]$ wurde eine klare Oberflächenanreicherung von $[Pf_2N]^-$ gegenüber Iodid beobachtet; dies kann durch die hohe Oberflächenaktivität von perfluorierten Alkylgruppen erklärt werden. Dagegen wurde bei äquimolaren Mischungen zweier ILs, die aus dem gleichen Anion und unterschiedlichen kationischen Kopfgruppen aufgebaut sind, nur eine geringe Oberflächenanreicherung (von $[P_{4441}]^+$ im Fall der $[P_{4441}][MeOSO_3]/[C_8C_1Im][MeOSO_3]$-Mischung) bzw. eine homogene Verteilung der Kationen (im Fall der $[S(CH_3)_3][Tf_2N]/[C_2C_1Im][Tf_2N]$-Mischung) beobachtet.

Ein klarer Einfluss koordinierender Liganden auf die Oberflächenaktivität von Übergangsmetallkomplexen zeigte sich bei Lösungen von katalytisch-aktiven Rh-Komplexen in $[C_2C_1Im][EtOSO_3]$: Während $[Rh(acac)(CO)_2]$ an sich keine Oberflächenaktivität in der IL aufwies, wurde durch Zugabe von $[Rh(acac)(CO)_2]$ in eine Lösung von Na_3tppts in $[C_2C_1Im][EtOSO_3]$ mindestens ein CO-Ligand durch einen tppts Liganden ausgetauscht. Dieser Ligand reicherte sich selbst bereits stark an der Oberfläche von $[C_2C_1Im][EtOSO_3]$ an. Durch die Einführung des oberflächenaktiven tppts-Liganden in den Rh-Komplex wird die

Oberflächenaktivität des Rh-Komplexes gesteigert, was zu einem Überschuss des Rh(tppts)-Komplexes an der Oberfläche führt.

Verfolgung von Reaktionen in flüssiger Phase mit in situ XPS

Aufgrund der sogenannten „chemischen Verschiebung“, d.h. durch den Einfluss der chemischen Umgebung und des Oxidationszustandes eines Atoms auf die Bindungsenergie seiner Rumpfniveau-Elektronen, lassen sich Reaktionen mit *in situ* XPS erfassen. In dieser Arbeit wurde zum ersten Mal demonstriert, dass sich auch klassische organische Reaktionen in der flüssigen Phase verfolgen lassen, wenn man die chemisch reaktiven Gruppen kovalent mit ionischen Kopfgruppen von ILs verknüpft. Bei der untersuchten Reaktion zwischen $[(Me_2NC_3H_6)C_1Im][TfO]$ und $[C_2C_1Im][ClC_4H_8SO_3]$ wurde das kovalent gebundene Chlor durch die tertiäre Amingruppe substituiert, wobei Chlorid und eine Ammoniumgruppe entstanden. Die Veränderungen der Ladungen am Chlor und Stickstoff verursachten eine eindeutige Verschiebung der Bindungsenergie in der Cl 2p und N 1s Region. Die quantitative Auswertung ergab, dass unter den UHV Bedingungen nur ~56% der $[ClC_4H_8SO_3]^-$ Anionen innerhalb der Substitutionsreaktion umgesetzt wurden. Als Parallelreaktionen wurden die Bildung eines anionischen Sulfonatesters und die intramolekulare Eliminierung eines flüchtigen Sultons aus dem $[ClC_4H_8SO_3]^-$ Anion identifiziert.

Auch Röntgenstrahlungs-induzierte Oxidations- und Reduktionsprozesse konnten mittels *in situ* XPS untersucht werden. Im Mittelpunkt stand dabei die röntgeninduzierte Reduktion des Pt^{IV}-Komplexes $[Pt^{IV}Cl_6]^{2-}$ in $[C_2C_1Im][EtOSO_3]$ und $[C_2C_1Im][Tf_2N]$. Während in $[C_2C_1Im][EtOSO_3]$ eine komplette Reduktion des $[Pt^{IV}Cl_6]^{2-}$ Komplexes zu Pt^{II} beobachtet wurde, erfolgte die Reduktion des Pt^{IV} in $[C_2C_1Im][Tf_2N]$ nur zu etwa 30%. Dies lässt vermuten, dass das IL Anion eine entscheidende Rolle im Reduktionsprozess einnimmt. Untersuchungen von Shkrob *et al.* zeigten, das Radikale, welche durch die Reaktion von Elektronen mit $[Tf_2N]^-$ entstehen, hauptsächlich durch Rekombination zerfallen, während die Reaktion zwischen $[EtOSO_3]^-$ und Elektronen hauptsächlich zu $CH_3{}^{\bullet}CHOH$ Radikalen führt, welche imstande sind den $[Pt^{IV}Cl_6]^{2-}$ Komplex zu reduzieren.[110]

Als letzter Reaktionstyp wurde schließlich die Wechselwirkung von NH_3 aus der Gasphase mit der IL $[C_8C_1Im][Cu^{II}Cl_3]$ mit *in situ* XPS modellhaft untersucht. Bei einer Probentemperatur von ~90 K erfolgte die Multilagenadsorption des NH_3 auf der (gefrorenen) IL-Probe. Nach Desorption der Multilage bis etwa 125 K verblieb ein dünne Schicht NH_3 auf der Probe zurück. Geringe Mengen des NH_3 konnten auch noch nach Heizen auf eine Probentemperatur von ~224 K beobachtet werden, wobei sich die Probe im flüssigen Zustand

befand. Eine komplette Desorption des NH_3 erfolgte schließlich bei ~245 K. Die Analyse des Cu $2p_{3/2}$ Signals zeigte Veränderungen der Satellitenstruktur nach NH_3-Adsorption, was auf eine chemisorbierte NH_3-Spezies hinwies.

7. Literature

[1] H. Weingärtner, *Angew. Chem., Int. Ed.* **2008**, *47*, 654.
[2] R. P. Swatloski, R. D. Rogers, J. D. Holbrey, *Dissolution and processing of cellulose using ionic liquids*, *Int. Pat*., WO 03/029329, **2003**.
[3] C. P. Fredlake, J. M. Crosthwaite, D. G. Hert, S. N. V. K. Aki, J. F. Brennecke, *J. Chem. Eng. Data* **2004**, *49*, 954.
[4] M. J. Earle, J. Esperanca, M. A. Gilea, J. N. C. Lopes, L. P. N. Rebelo, J. W. Magee, K. R. Seddon, J. A. Widegren, *Nature* **2006**, *439*, 831.
[5] P. Wasserscheid, *Nature* **2006**, *439*, 797.
[6] D. M. Fox, J. W. Gilman, A. B. Morgan, J. R. Shields, P. H. Maupin, R. E. Lyon, H. C. De Long, P. C. Trulove, *Ind. Eng. Chem. Res.* **2008**, *47*, 6327.
[7] F. Endres, S. Z. El Abedin, *Phys. Chem. Chem. Phys.* **2006**, *8*, 2101.
[8] A. J. Carmichael, K. R. Seddon, *J. Phys. Org. Chem.* **2000**, *13*, 591.
[9] R. Giernoth, *Angew. Chem., Int. Ed.* **2010**, *49*, 2834.
[10] P. Wasserscheid, T. Welton, *Ionic liquids in synthesis*, 2nd ed., Wiley-VCH, Weinheim, **2008**.
[11] T. Welton, *Coord. Chem. Rev.* **2004**, *248*, 2459.
[12] T. Welton, J. P. Hallett, *Chem. Rev.* **2011**, *111*, 3508.
[13] D. R. MacFarlane, M. Forsyth, P. C. Howlett, J. M. Pringle, J. Sun, G. Annat, W. Neil, E. I. Izgorodina, *Acc. Chem. Res.* **2007**, *40*, 1165.
[14] J. L. Anderson, D. W. Armstrong, G. T. Wei, *Anal. Chem.* **2006**, *78*, 2892.
[15] F. Zhou, Y. M. Liang, W. M. Liu, *Chem. Soc. Rev.* **2009**, *38*, 2590.
[16] A. Berthod, M. Ruiz-Angel, S. Carda-Broch, *J. Chromatogr., A* **2008**, *1184*, 6.
[17] M. Maase, K. Massonne, *Ionic Liquids IIIb: Fundamentals, Progress, Challenges and Opportunities: Transformations and Processes* **2005**, *902*, 126.
[18] C. P. Mehnert, R. A. Cook, N. C. Dispenziere, M. Afeworki, *J. Am. Chem. Soc.* **2002**, *124*, 12932.
[19] A. Riisager, R. Fehrmann, M. Haumann, B. S. K. Gorle, P. Wasserscheid, *Ind. Eng. Chem. Res.* **2005**, *44*, 9853.
[20] T. J. Gannon, G. Law, P. R. Watson, A. J. Carmichael, K. R. Seddon, *Langmuir* **1999**, *15*, 8429.
[21] G. Law, P. R. Watson, A. J. Carmichael, K. R. Seddon, B. Seddon, *Phys. Chem. Chem. Phys.* **2001**, *3*, 2879.
[22] C. Hardacre, *Annu. Rev. Mater. Res.* **2005**, *35*, 29.
[23] S. Hüfner, *Photoelectron Spectroscopy*, Springer-Verlag, Berlin Heidelberg, **1995**.
[24] J. N. A. C. Lopes, A. A. H. Padua, *J. Phys. Chem. B* **2006**, *110*, 3330.
[25] Y. T. Wang, G. A. Voth, *J. Am. Chem. Soc.* **2005**, *127*, 12192.
[26] G. D. Smith, O. Borodin, L. Y. Li, H. Kim, Q. Liu, J. E. Bara, D. L. Gin, R. Nobel, *Phys. Chem. Chem. Phys.* **2008**, *10*, 6301.
[27] Z. F. Fei, W. H. Ang, D. B. Zhao, R. Scopelliti, E. E. Zvereva, S. A. Katsyuba, P. J. Dyson, *J. Phys. Chem. B* **2007**, *111*, 10095.
[28] H. Hoffmann, J. Wurtz, *J. Mol. Liq.* **1997**, *72*, 191.
[29] M. Monduzzi, *Curr. Opin. Colloid Interface Sci.* **1998**, *3*, 467.
[30] M. Hasib-ur-Rahman, M. Siaj, F. Larachi, *Chem. Eng. Process.* **2010**, *49*, 313.
[31] D. J. Tempel, P. B. Henderson, J. R. Brzozowski, R. M. Pearlstein, H. S. Cheng, *J. Am. Chem. Soc.* **2008**, *130*, 400.
[32] T. Cremer, PhD Thesis, Fredrich-Alexander-University Erlangen-Nuremberg, **2012**.
[33] D. Briggs, M. P. Seah, *Practical Surface Analysis*, Springer-Verlag, Berlin, **1990**.
[34] M. P. Seah, W. A. Dench, *Surf. Interface Anal.* **1979**, *1*, 2.
[35] R. F. Roberts, D. L. Allara, C. A. Pryde, D. N. E. Buchanan, N. D. Hobbins, *Surf. Interface Anal.* **1980**, *2*, 5.

[36] M. Probst, PhD Thesis, Friedrich-Alexander-University Erlangen-Nuremberg, **2003**.
[37] F. Grellner, PhD Thesis, Friedrich-Alexander-University Erlangen-Nuremberg, **1993**.
[38] M. Stark, Master Thesis, Friedrich-Alexander-University of Erlangen-Nuremberg, **2010**.
[39] C. D. Wagner, L. E. Davis, M. V. Zeller, J. A. Taylor, R. H. Raymond, L. H. Gale, *Surf. Interface Anal.* **1981**, *3*, 211.
[40] I. Langmuir, *Chem. Rev.* **1930**, *6*, 451.
[41] I. Langmuir, *Surface Chemistry (nobel lecture, 1932)*, Elsevier Publishing Company, Amsterdam, **1966**.
[42] P. B. Miranda, Y. R. Shen, *J. Phys. Chem. B* **1999**, *103*, 3292.
[43] S. Baldelli, *J. Phys. Chem. B* **2003**, *107*, 6148.
[44] T. Iimori, T. Iwahashi, H. Ishii, K. Seki, Y. Ouchi, R. Ozawa, H. Hamaguchi, D. Kim, *Chem. Phys. Lett.* **2004**, *389*, 321.
[45] C. S. Santos, S. Baldelli, *J. Phys. Chem. B* **2009**, *113*, 923.
[46] J. Penfold, *Rep. Prog. Phys.* **2001**, *64*, 777.
[47] P. Lang, *J. Phys.: Condens. Matter* **2004**, *16*, R699.
[48] Y. Jeon, J. Sung, W. Bu, D. Vaknin, Y. Ouchi, D. Kim, *J. Phys. Chem. C* **2008**, *112*, 19649.
[49] J. Bowers, M. C. Vergara-Gutierrez, J. R. P. Webster, *Langmuir* **2004**, *20*, 309.
[50] E. Solutskin, B. M. Ocko, L. Taman, I. Kuzmenko, T. Gog, M. Deutsch, *J. Am. Chem. Soc.* **2005**, *127*, 7796.
[51] Y. F. Yano, H. Yamada, *Anal. Sci.* **2008**, *24*, 1269.
[52] W. Jiang, Y. T. Wang, T. Y. Yan, G. A. Voth, *J. Phys. Chem. C* **2008**, *112*, 1132.
[53] W. Jiang, T. Y. Yan, Y. T. Wang, G. A. Voth, *J. Phys. Chem. B* **2008**, *112*, 3121.
[54] R. M. Lynden-Bell, M. Del Popolo, *Phys. Chem. Chem. Phys.* **2006**, *8*, 949.
[55] K. R. J. Lovelock, I. J. Villar-Garcia, F. Maier, H. P. Steinrück, P. Licence, *Chem. Rev.* **2010**, *110*, 5158.
[56] H. P. Steinrück, *Phys. Chem. Chem. Phys.* **2012**, *14*, 5010.
[57] E. F. Smith, I. J. Villar Garcia, D. Briggs, P. Licence, *Chem. Commun.* **2005**, 5633.
[58] V. Lockett, R. Sedev, C. Bassell, J. Ralston, *Phys. Chem. Chem. Phys.* **2008**, *10*, 1330.
[59] O. Höfft, S. Bahr, M. Himmerlich, S. Krischok, J. A. Schaefer, V. Kempter, *Langmuir* **2006**, *22*, 7120.
[60] S. Krischok, M. Eremtchenko, M. Himmerlich, P. Lorenz, J. Uhlig, A. Neumann, R. Ottking, W. J. D. Beenken, O. Hofft, S. Bahr, V. Kempter, J. A. Schaefer, *J. Phys. Chem. B* **2007**, *111*, 4801.
[61] D. Yoshimura, T. Yokoyama, T. Nishi, H. Ishii, R. Ozawa, H. Hamaguchi, K. Seki, *J. Electron Spectrosc. Relat. Phenom.* **2005**, *144*, 319.
[62] K. Kanai, T. Nishi, T. Iwahashi, Y. Ouchi, K. Seki, Y. Harada, S. Shin, *J. Chem. Phys.* **2008**, *129*, 224507.
[63] T. Nishi, T. Iwahashi, H. Yamane, Y. Ouchi, K. Kanai, K. Seki, *Chem. Phys. Lett.* **2008**, *455*, 213.
[64] K. Kanai, T. Nishi, T. Iwahashi, Y. Ouchi, K. Seki, Y. Harada, S. Shin, *J. Electron Spectrosc. Relat. Phenom.* **2009**, *174*, 110.
[65] S. Caporali, U. Bardi, A. Lavacchi, *J. Electron Spectrosc. Relat. Phenom.* **2006**, *151*, 4.
[66] E. F. Smith, F. J. M. Rutten, I. J. Villar-Garcia, D. Briggs, P. Licence, *Langmuir* **2006**, *22*, 9386.
[67] T. Hammer, M. Reichelt, H. Morgner, *Phys. Chem. Chem. Phys.* **2010**, *12*, 11070.
[68] K. Nakajima, A. Ohno, H. Hashimoto, M. Suzuki, K. Kimura, *J. Chem. Phys.* **2010**, *133*, 044702.
[69] K. Nakajima, A. Ohno, M. Suzuki, K. Kimura, *Langmuir* **2008**, *24*, 4482.
[70] M. Tariq, A. P. Serro, J. L. Mata, B. Saramago, J. M. S. S. Esperanca, J. N. C. Lopes, L. P. N. Rebelo, *Fluid Phase Equilib.* **2010**, *294*, 131.
[71] C. L. Yaws, *Chemical Properties Handbook*, McGraw-Hill, New York, **1999**.
[72] T. Koddermann, D. Paschek, R. Ludwig, *ChemPhysChem* **2008**, *9*, 549.
[73] S. S. Jaswal, T. P. Sharma, *J. Phys. Chem. Solids* **1973**, *34*, 509.
[74] F. Hajj, *J. Chem. Phys.* **1966**, *44*, 4618.
[75] I. M. Boswarva, C. S. N. Murthy, *J. Phys. Chem. Solids* **1981**, *42*, 109.

[76] A. Deyko, K. R. J. Lovelock, J. A. Corfield, A. W. Taylor, P. N. Gooden, I. J. Villar-Garcia, P. Licence, R. G. Jones, V. G. Krasovskiy, E. A. Chernikova, L. M. Kustov, *Phys. Chem. Chem. Phys.* **2009**, *11*, 8544.
[77] B. E. Smart, *J. Fluorine Chem.* **2001**, *109*, 3.
[78] R. H. Boyd, L. Kesner, *J. Chem. Phys.* **1980**, *72*, 2179.
[79] Q. Zhou, W. A. Henderson, G. B. Appetecchi, S. Passerini, *J. Phys. Chem. C* **2010**, *114*, 6201.
[80] M. Montanino, M. Moreno, F. Alessandrini, G. B. Appetecchi, S. Passerini, Q. Zhou, W. A. Henderson, *Electrochim. Acta* **2012**, *60*, 163.
[81] F. Castiglione, G. Raos, G. B. Appetecchi, M. Montanino, S. Passerini, M. Moreno, A. Famulari, A. Mele, *Phys. Chem. Chem. Phys.* **2010**, *12*, 1784.
[82] B. Dong, N. Li, L. Q. Zheng, L. Yu, T. Inoue, *Langmuir* **2007**, *23*, 4178.
[83] J. Bowers, C. P. Butts, P. J. Martin, M. C. Vergara-Gutierrez, R. K. Heenan, *Langmuir* **2004**, *20*, 2191.
[84] R. Souda, *Surf. Sci.* **2010**, *604*, 1694.
[85] S. Thomaier, W. Kunz, *J. Mol. Liq.* **2007**, *130*, 104.
[86] N. Li, S. H. Zhang, L. Q. Zheng, B. Dong, X. W. Li, L. Yu, *Phys. Chem. Chem. Phys.* **2008**, *10*, 4375.
[87] S. B. Velasco, M. Turmine, D. Di Caprio, P. Letellier, *Colloids Surf. A* **2006**, *275*, 50.
[88] L. Shi, M. Zhao, L. Zheng, *Colloids Surf. A* **2011**, *392*, 305.
[89] Q. H. Zhang, S. M. Liu, Z. P. Li, J. Li, Z. J. Chen, R. F. Wang, L. J. Lu, Y. Q. Deng, *Chem. Eur. J.* **2009**, *15*, 765.
[90] T. Cremer, C. Kolbeck, K. J. R. Lovelock, N. Paape, R. Wolfel, P. S. Schulz, P. Wasserscheid, H. Weber, J. Thar, B. Kirchner, F. Maier, H. P. Steinrück, *Chem. Eur. J.* **2010**, *16*, 9018.
[91] F. P. Pruchnik, P. Smolenski, K. Wajda-Hermanowicz, *J. Organomet. Chem.* **1998**, *570*, 63.
[92] N. Sieffert, G. Wipff, *J. Phys. Chem. B* **2007**, *111*, 4951.
[93] N. Sieffert, G. Wipff, *J. Phys. Chem. C* **2008**, *112*, 6450.
[94] K. R. J. Lovelock, E. F. Smith, A. Deyko, I. J. Villar-Garcia, P. Licence, R. G. Jones, *Chem. Commun.* **2007**, 4866.
[95] F. L. Qiu, A. W. Taylor, S. Men, I. J. Villar-Garcia, P. Licence, *Phys. Chem. Chem. Phys.* **2010**, *12*, 1982.
[96] A. W. Taylor, F. L. Qiu, I. J. Villar-Garcia, P. Licence, *Chem. Commun.* **2009**, 5817.
[97] R. Wibowo, L. Aldous, R. M. J. Jacobs, N. S. A. Manan, R. G. Compton, *Chem. Phys. Lett.* **2011**, *517*, 103.
[98] R. Wibowo, L. Aldous, R. M. J. Jacobs, N. S. A. Manan, R. G. Compton, *Chem. Phys. Lett.* **2011**, *509*, 72.
[99] D. Weingarth, A. Foelske-Schmitz, A. Wokaun, R. Kötz, *Electrochem. Commun.* **2011**, *13*, 619.
[100] M. Sobota, M. Schmid, M. Happel, M. Amende, F. Maier, H. P. Steinrück, N. Paape, P. Wasserscheid, M. Laurin, J. M. Gottfried, J. Libuda, *Phys. Chem. Chem. Phys.* **2010**, *12*, 10610.
[101] A. W. Adamson, W. L. Waltz, E. Zinato, D. W. Watts, P. D. Fleischauer, R. D. Lindholm, *Chem. Rev.* **1968**, *68*, 541.
[102] P. Burroughs, A. Hamnett, J. F. Mcgilp, A. F. Orchard, *J. Chem. Soc., Faraday Trans. 2* **1975**, *71*, 177.
[103] A. Katrib, *J. Electron Spectrosc. Relat. Phenom.* **1980**, *18*, 275.
[104] C. Kolbeck, T. Cremer, K. R. J. Lovelock, N. Paape, P. S. Schulz, P. Wasserscheid, F. Maier, H. P. Steinrück, *J. Phys. Chem. B* **2009**, *113*, 8682.
[105] N. Paape, W. Wei, A. Bosmann, C. Kolbeck, F. Maier, H. P. Steinrück, P. Wasserscheid, P. S. Schulz, *Chem. Commun.* **2008**, 3867.
[106] R. Streber, C. Papp, M. P. A. Lorenz, A. Bayer, R. Denecke, H. P. Steinrück, *Angew. Chem., Int. Ed.* **2009**, *48*, 9743.
[107] A. Keppler, M. Himmerlich, T. Ikari, M. Marschewski, E. Pachomow, O. Hofft, W. Maus-Friedrichs, F. Endres, S. Krischok, *Phys. Chem. Chem. Phys.* **2011**, *13*, 1174.
[108] L. E. Cox, D. M. Hercules, *J. Electron. Spectrosc. Relat. Phenom.* **1972/73**, *1*, 193.
[109] S. O. Grim, L. J. Matienzo, W. E. Swartz, *Inorg. Chem.* **1974**, *13*, 447.

[110] I. A. Shkrob, T. W. Marin, S. D. Chemerisov, J. F. Wishart, *J. Phys. Chem. B* **2011**, *115*, 3872.
[111] V. I. Nefedov, Y. V. Salyn, *Inorg. Chim. Acta* **1978**, *28*, L135.
[112] D. Heß, M. Gorlov, A. Fischer, L. Kloo, *Z. Anorg. Allg. Chem.* **2007**, *633*, 643.
[113] T. G. Appleton, J. R. Hall, S. F. Ralph, C. S. M. Thompson, *Inorg. Chem.* **1984**, *23*, 3521.
[114] Y. F. Hu, Z. C. Liu, C. M. Xu, X. M. Zhang, *Chem. Soc. Rev.* **2011**, *40*, 3802.
[115] F. Karadas, M. Atilhan, S. Aparicio, *Energy Fuels* **2010**, *24*, 5817.
[116] A. Yokozeki, M. B. Shiflett, *Ind. Eng. Chem. Res.* **2007**, *46*, 1605.
[117] W. Shi, E. J. Maginn, *AIChE J.* **2009**, *55*, 2414.
[118] J. Huang, A. Riisager, R. W. Berg, R. Fehrmann, *J. Mol. Cat. A: Chem.* **2008**, *279*, 170.
[119] G. van der Laan, C. Westra, C. Haas, G. A. Sawatzky, *Phys. Rev. B* **1981**, *23*, 4369.
[120] N. S. McIntyre, M. G. Cook, *Anal. Chem.* **1975**, *47*, 2208.

8. Acknowledgement

At this point, I would like to express my gratitude to several persons.

Prof. Hans-Peter Steinrück:
For giving me the opportunity to do my PhD thesis in his group, for his support and the constructive discussions.

Dr. Florian Maier:
For his guidance and his encouragement; for the scientific discussions and his substantial ideas.

Till Cremer:
I couldn't have wished for another co-worker. The last 4-5 years were trouble-free and I really appreciated working with him.

Ionic Liquid Surface Science (ILSS) group:
Thanks goes to my other co-workers in the ILSS project, namely Dr. Kevin J. R. Lovelock, Dr. Alexey Deyko, Florian Rietzler and especially Inga Niedermaier. Furthermore, I would like to thank Nina Zeilmann and Uwe Göbel for their experimental contributions within their Bachelor theses.

Prof. Peter Wasserscheid and his group members:
For the productive discussions, fruitful ideas and the provided ILs. Special recognition is given to Natalie Paape and Nicola Taccardi, who synthesised most of the ILs studied in this work.

Cooperation partners:
I would like to thank Julia Lehmann and Prof. Andreas P. Fröba for the surface tension and density measurements and Jing Li and Prof. Thomas Drewello for the ESI-MS measurements.

Technical Support:
The downtime of the XPS chamber would have been at least double as long, if it hadn't been for the technical staff. Therefore, I'm very grateful to Bernd Kress, Hans-Peter Bäumler and Friedhold Wölfel and his co-workers.

PC II members:
For a wonderful working atmosphere.

9. Appendix

[P1] K. R. J. Lovelock, **C. Kolbeck**, T. Cremer, N. Paape, P. S. Schulz, P. Wasserscheid, F. Maier, H.-P. Steinrück
Influence of Different Substituents on the Surface Composition of Ionic Liquids Studied Using ARXPS
J. Phys. Chem. B 113 (2009) 2854-2864.

[P2] F. Maier, T. Cremer, **C. Kolbeck**, K. R. J. Lovelock, N. Paape, P. S. Schulz, P. Wasserscheid, H.-P. Steinrück
Insights into the Surface Composition and Enrichment Effects of Ionic Liquids and Ionic Liquid Mixtures
Phys. Chem. Chem. Phys. 12 (2010) 1905-1915.

[P3] **C. Kolbeck**, J. Lehmann, K. R. J. Lovelock, T. Cremer, N. Paape, P. Wasserscheid, A. P. Fröba, F. Maier, H.-P. Steinrück
Density and Surface Tension of Ionic Liquids
J. Phys. Chem. B 114 (2010) 17025-17036.

[P4] **C. Kolbeck**, N. Paape, T. Cremer, P. S. Schulz, F. Maier, H.-P. Steinrück, P. Wasserscheid
Ligand Effects on the Surface Composition of Rh-Containing Ionic Liquid Solutions Used in Hydroformylation Catalysis
Chem. Eur. J. 16 (2010) 12083-12087.

[P5] **C. Kolbeck**, I. Niedermaier, N. Taccardi, P. S. Schulz, F. Maier, P. Wasserscheid, H.-P. Steinrück
Monitoring of Liquid-Phase Organic Reactions by Photoelectron Spectroscopy
Angew. Chem. Int. Ed. 51 (2012) 2610-2613.

[P6] I. Niedermaier, **C. Kolbeck**, N. Taccardi, P. S. Schulz, J. Li, T. Drewello, P. Wasserscheid, H.-P. Steinrück, F. Maier
Organic Reactions in Ionic Liquids Studied by in Situ XPS
ChemPhysChem 13 (2012) 1725-1735.

[P7] **C. Kolbeck**, N. Taccardi, N. Paape, P. S. Schulz, P. Wasserscheid, H.-P. Steinrück, F. Maier
Redox chemistry, solubility, and surface distribution of Pt(II) and Pt(IV) complexes dissolved in ionic liquids
J. Mol. Liq. doi:10.1016/j.molliq.2013.07.007.